Quaternary and Pliocene sea-level changes at Camarones, central Patagonia, Argentina

Karla Rubio-Sandoval [a,*], Deirdre D. Ryan [b], Sebastian Richiano [c], Luciana M. Giachetti [c], Andrew Hollyday [d], Jordon Bright [e], Evan J. Gowan [f,g], Marta Pappalardo [b], Jacqueline Austermann [d], Darrell S. Kaufman [e], Alessio Rovere [a,h]

[a] MARUM, Center for Marine Environmental Sciences, University of Bremen, Bremen, Germany
[b] Department of Earth Sciences, University of Pisa, Pisa, Italy
[c] National Scientific and Technical Research Council, Instituto Patagónico de Geología y Paleontología, Puerto Madryn, Argentina
[d] Lamont-Doherty Earth Observatory, Columbia University, New York, USA
[e] Northern Arizona University, Flagstaff, Arizona, USA
[f] Department of Earth and Environmental Sciences, Kumamoto University, Kumamoto, Japan
[g] KIKAI Institute for Coral Reef Sciences, Kagoshima, Japan
[h] DAIS, Department for Environmental Sciences, Statistics and Informatics, Ca' Foscari University of Venice, Venice, Italy

ARTICLE INFO

ABSTRACT

Geological indicators of past relative sea level changes are fundamental to reconstruct the extent of former ice sheet during past interglacials, which are considered analogs for future climate conditions. Four interglacials, dating from Holocene to Pliocene, have left sea-level imprints in the proximity of the coastal town of Camarones in Central Patagonia, Argentina. Sea-level index points were preserved as beach ridges deposited by storm waves above modern sea level. We used highly accurate survey techniques to measure the elevation of these deposits. Satellite derived wave measurements and wave runup models were then employed to calculate their indicative meaning (i.e., their elevation with respect to sea level at the time of deposition). The paleo relative sea levels (i. e., uncorrected for post-depositional vertical land motions) associated with the four interglacials (with $\pm 1\sigma$ uncertainties) are 6 ± 1.5 m (late Holocene); 8.7 ± 2.1 m (MIS 5e); 14.5 ± 1.5 m (MIS 9 or 11); and 36.2 ± 2.7 m (Early Pliocene). Ages have been obtained using both published (U-series, Electron Spin Resonance, and Radiocarbon) and new (Amino Acid Racemization and Radiocarbon) dating constraints. We compare our results with published glacial isostatic adjustment and mantle dynamic topography predictions, and we highlight that refining these models before calculating the global mean sea level for the interglacials mentioned above is necessary. Our high-resolution sea-level index points serve as an important contribution to the record of paleo relative sea-level in the Southwestern Atlantic.

1. Introduction

Several past interglacials were characterized by global average temperatures warmer than pre-industrial, which resulted in smaller ice sheets and higher ocean volumes (Dutton et al., 2015). Geological records from several sites around the globe provide hard evidence that local sea levels during such periods were higher than today (Siddall et al., 2007; Raymo et al., 2011; Rovere et al., 2023). Reconstructing global mean sea levels (GMSL) that characterize earlier interglacials helps to constrain models of polar ice melting in the near future (Gilford et al., 2020; DeConto et al., 2021) and ultimately lead to a better understanding of the physics that drive high-end melting scenarios (van de Wal et al., 2022).

The Quaternary sea-level highstands have been studied at several locations on the world's coasts and continental shelves via both direct and indirect proxies. In general, the availability of direct proxies decreases with the age of the highstand (Khan et al., 2019a), which makes GMSL during early Quaternary and Pliocene interglacials more difficult to quantify. Further, direct proxies only measure relative sea level (RSL), still uncorrected for uplift or subsidence that may be caused by different

---

processes such as Glacial Isostatic Adjustment (GIA), mantle Dynamic Topography (DT) and tectonics (Rovere et al., 2016).

Interglacial peak sea level differs during the last 5 Myr in both magnitude and duration. During the Pliocene (~5.3–2.5 Ma), global temperatures were up to 4 °C higher than pre-industrial (Fedorov et al., 2013), and GMSL oscillated by tens of meters (Grant et al., 2019), with proxies suggesting that sea-level highstands were around 17 m higher than present in the mid-Pliocene (~3 Ma) and around 25 m higher in the Early Pliocene Climatic Optimum (~5 Ma, Dumitru et al., 2019). Pliocene ice models suggest that, during the warmest interglacials of this geological epoch, Greenland was ice-free, and the West Antarctic ice sheet was likely subject to periodic collapses (Naish et al., 2009; Solgaard et al., 2011).

Regarding Quaternary highstands, several sites carry information on sea level during MIS 11c (424–395 ka, Hearty et al., 1999; Murray-Wallace, 2002; Olson and Hearty, 2009; Bowen, 2010; Roberts et al., 2012) an unusually long interglacial with high carbon dioxide levels (Tzedakis et al., 2022). Direct proxies, corrected for GIA and vertical land motions, suggest that MIS 11c GMSL was 8–11.5 m (Chen et al., 2014) or 6–13 m (Raymo and Mitrovica, 2012) above present. GMSL during MIS 9 (~331-310 ka) was reported close to the present-day sea level (Murray-Wallace, 2002; Siddall et al., 2007).

Evidence of Late Quaternary interglacials is more ubiquitous, with thousands of sites dated to MIS 5 (in particular MIS 5e, ~125 ka, Rovere et al., 2023). In the AR6 IPCC REPORT, Gulev et al. (2021) remark that sea level was "5–10 m (likely) higher during the Last Interglacial (125, 000 years ago)". Recent works suggest that MIS 5e GMSL was instead generally lower than 5 m, but still higher than present (Polyak et al., 2018; Clark et al., 2020; Dyer et al., 2021; Dumitru et al., 2023). Sea level during other stages of MIS 5, namely MIS 5c (~100 ka) and MIS 5a (~80 ka), is generally reported to have peaked from few tens of meters below up to close to present-day sea level (Muhs et al., 2012; Simms et al., 2016; Creveling et al., 2017; Thompson and Creveling, 2021; Tawil-Morsink et al., 2022; Marra et al., 2023).

During the current interglacial (~6 ka to present), Gulev et al. (2021) report that "*there is medium confidence that GMSL was within –3.5 to +0.5 m (very likely) of present during the mid-Holocene (6000 years ago)*". For which concerns the source of melting, Fox-Kemper et al. (2021) states that "*[…] GMSL rise slowed coincidently with final melting of the Laurentide ice sheet by 6.7 ± 0.4 ka […], after which only Greenland and Antarctic ice sheets could have contributed significantly*". This seems in line with recent work based on a global database of sea-level index points (Khan et al., 2019b) showing that it is likely that GMSL was higher (up to 1.5 m) than today during the mid-Holocene with a significant contribution of excess melt coming from the Antarctic ice sheet (Creel et al., 2023).

To reduce uncertainties on estimates of GMSL during past interglacials, it is essential to provide field constraints that have reliable chronological attribution, are precisely measured and have a quantifiable relationship to past sea level (i.e, indicative meaning, Shennan, 2015). Moreover, locations at passive margins that have preserved multiple highstands give an opportunity to better quantify post-depositional vertical land motions, as they are less subject to these effects (e.g., subduction or uplift during successive earthquake cycles, Yousefi et al., 2020).

Much of the Southern part of the Atlantic Ocean is a passive margin, and coastal deposits associated with past interglacials shape the morphology of the coastal landscape and record the history of relative sea level change after deglaciation (see review works by Gowan et al., 2021a; Rubio-Sandoval et al., 2021). In this study, we present new data detailing Quaternary sea-level changes at Camarones, Central Patagonia, Argentina. We provide new survey data and a new way of estimating the indicative meaning of beach ridges. We couple the results with

dating on mollusk shells via Amino Acid Racemization. Building upon previously published stratigraphic data and radiometric ages, as well as GIA and DT models, we discuss possible GMSL inferences during past warm periods.

2. Study area

The Patagonia coastline of Argentina has been a target area for sea-level research for at least four decades (Bayarsky and Codignotto, 1982; Codignotto, 1983; Rutter et al., 1989) due to the exceptional preservation of geological records associated with former sea levels and for its location that makes it sensitive to isostatic rebound following the waxing and waning of the WestAntarctic ice sheet (Rostami et al., 2000; Milne et al., 2005; Gowan et al., 2021a). Numerous works describe in detail the geomorphology and stratigraphic subdivision of the elevated littoral deposits along the coastlines of Patagonia (see an extensive review by Pedoja et al., 2011). One of the most complete descriptions of these deposits derives from the work of Feruglio (1949), who described six marine terrace systems based on their elevation and mollusk fauna. The elevation of these marine deposits ranges from 8 to 186 m above mean sea level. Along the shore, the presence of beach ridges at varying heights is also conspicuous, enough so that it was noted by Charles Darwin during his voyage on the Beagle vessel (Darwin, 1851).

Patagonian beach ridge deposits are typically composed of a sandy gravel matrix, rich in pebbles and mollusk shells (Schellmann and Radtke, 2000) and are - from a geomorphological standpoint - raised storm berms created by the deposition of sediments by wave runup. Different dating techniques have been employed to determine the age of these deposits: radiocarbon, U-series, Electron Spin Resonance and Strontium Isotope Stratigraphy (Schellmann and Radtke, 2000; Pappalardo et al., 2015; Rovere et al., 2020).

The small town of Camarones (Chubut Province, Argentina) lies at the northern end of the San Jorge Gulf, ~1300 km south of Buenos Aires (Fig. 1). It is located on a passive margin and is embedded within the South America Plate, over 1000 km north of the boundary with the Scotia plate. In proximity of Camarones, several authors reported relic beach ridges, emplaced by sea level during the Quaternary (Codignotto et al., 1992; Schellmann and Radtke, 2000, 2003, 2007, 2010; Ribolini et al., 2011; Zanchetta et al., 2012; Pappalardo et al., 2015; Bini et al., 2018) and the Pliocene (Feruglio, 1949; Del Río et al., 2013; Rovere et al., 2020). While located on a passive margins, these paleo shorelines were subject to substantial vertical land motions due to both glacial isostatic adjustment (Mitrovica et al., 2001; Peltier, 2002) in response to polar ice melting and, on longer time scales (hundred of thousands to millions of years), mantle dynamic topography (Braun, 2010; Austermann et al., 2017), which led to significant uplift over the past ~5 million years (Hollyday et al., 2023).

3. Methods

3.1. Elevation measurement

The elevations of sea-level index points described in this study were measured using differential Global Navigation Satellite systems (GNSS). The elevation of the Pliocene sea-level index points was surveyed in 2014 with a Trimble ProXRT receiver with Tornado antenna, receiving OmniSTAR HP real-time corrections, as described in Rovere et al. (2020). During that campaign, preliminary surveys on both modern and middle/late Pleistocene shorelines in the area were carried out. Those data are reported in this work following the same GNSS processing methods described in Rovere et al. (2020).

Two further field campaigns, focussed on MIS 5 beach ridges and modern data, were carried out in November 2019 and April 2022. In
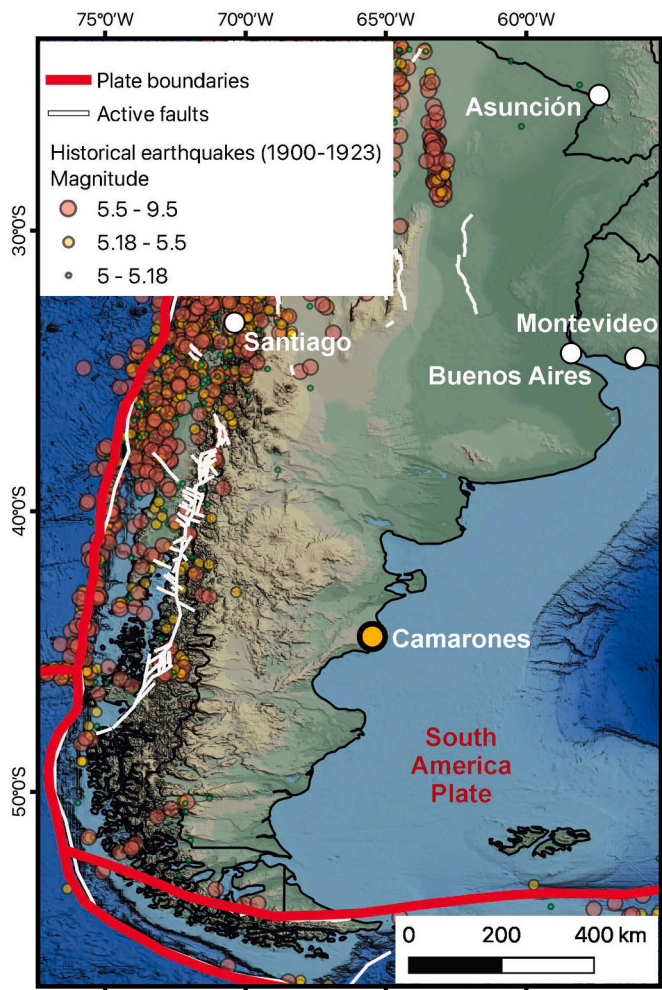
Fig. 1. Study area. Location of Camarones within the Southern part of South America. Credits: Base map from Ryan et al. (2009). Active faults from Styron (2019) and plate boundaries derived from Bird (2003), as modified by Hugo Ahlenius and Nordpil on GitHub (https://github.com/fraxen/tectonicplates). Historical earthquakes from US Geological Survey Earthquake Hazards Program, 2017.

these campaigns, GNSS surveys were performed using a single-band EMLID RS + GNSS composed of a base and a rover unit. In both campaigns, the base station was located on top of a pole with full view of the sky (Supplementary Figure 1A and B) and was left static collecting data for a variable amount of time including between 5 and 14 h over five separate deployments (Supplementary Table 1). The data collected from the base station were processed using the Precise Point Positioning service of the Natural Resources of Canada (NRCAN-PPP), and then averaged using the "GPS Utilities" scripts (Rovere, 2021). The results of the GNSS base processing are reported in Supplementary Table 1 and illustrated in Supplementary Figure 1C and D.

Once the base position and the associated positional errors were calculated, the rover data was processed using the Post Processed Kinematic (PPK) workflow in the software EMLID Studio. The collection of GNSS rover data was done in static mode for up to 10 min, depending on satellite visibility conditions. The workflow was validated by measuring twice (once in 2019 and once in 2022) a benchmark point called "GPS N°35" located in the proximity of the town of Camarones (Supplementary Figure 2A and B). The precise coordinates of this point are reported by the Argentinian "Instituto Geográfico Nacional" (National Geographical Institute), which measured it in 1995. There is a very good agreement between our vertical measurements and the benchmark ellipsoid elevation (Supplementary Figure 2 C). The

Northing and Easting coordinates of our GNSS survey appear internally consistent but shifted by about half meter (Supplementary Figure 2 D).

Data were originally recorded in WGS84 coordinates, with height above the ITRF2008 ellipsoid (these are the same datums to which the "GPS N°35" benchmark is referred). Orthometric heights (above mean sea level) were then calculated subtracting the GEOIDEAR16 geoid height from the measured ellipsoid height. It was estimated that the GEOIDEAR16 has an overall vertical accuracy of 0.1 m (Piñón et al., 2018). Pappalardo et al. (2019) has shown that, in some areas of Patagonia, referring GNSS data to the GEOIDEAR16 geoid might be affected by large discrepancies if compared with the sea level observed by tide gauge data. Therefore, we use two GNSS observations: one of instantaneous sea level and one of the high tide mark, to benchmark the GEOIDEAR16 geoid at this location. The results show that there is little to no discrepancy between observed elevations and tidal predicted values (Supplementary Fig. 3). In any case, we remark that all the GNSS data collected in this work are also originally referred to the ITRF2008 ellipsoid, and ellipsoid elevations are given in the supplementary material in case new datums become available in the future (see Supplementary Information for details).

The elevation error (σE) of each GNSS point surveyed in the field was calculated using the following formula:

$$\sigma E = \sqrt{GNSS_e^2 + Base_e^2 + Geoid_e^2 + Bench_e^2} \tag{1}$$

where $GNSS_e$ is the error given as output by the GNSS system, $Base_e$ (only for data collected in 2019 and 2022) is the elevation error of the base station (0.187 m), $Geoid_e$ is the error associated with the GEOIDEAR16 (0.1 m), and $Bench_e$ is the average of the absolute differences between the GNSS points and the benchmark "GPS N°35" (0.06 m).

In some instances, the same point or the same stratigraphic context within close points was measured during different campaigns. In these cases, elevations were averaged using the same processing scripts adopted for the base station described above (Rovere, 2021).

3.2. Calculating the indicative meaning

For each point measured in the field representative of a past sea-level position, it is necessary to quantify its relationship to the former sea level calculating the indicative meaning (Van de Plassche, 1986; Shennan, 2015). The indicative meaning is composed of the reference water level (RWL) and the indicative range (IR), which are calculated as follows:

$$RWL = \frac{U_l + L_l}{2} \tag{2}$$

$$IR = U_l - L_l \tag{3}$$

where U_l and L_l are, respectively, the upper and lower limits of occurrence of the same facies observed in the fossil record along the modern coast. Once RWL and IR are calculated, they are used to calculate paleo RSL and its associated uncertainty as follows:

$$RSL = E - RWL \tag{4}$$

$$\sigma_{RSL} = \sqrt{\sigma_E^2 + \left(\frac{IR}{2}\right)^2} \tag{5}$$

where E is the measured elevation, and σ_{RSL} and σ_E are the uncertainties of relative sea level and measured elevation, respectively.

For the Pliocene sea-level index points we maintained the indicative meaning quantified by Rovere et al. (2020). For Pleistocene deposits, we measured as a sea-level index point the top layer where articulated (not in living position, transported by lowenergy processes) *Ameghinomya antiqua* (formerly known as *Protothaca antiqua*) shells are present within the beach ridge. This benthic bivalve is typical of the Magellanic region (Gordillo, 1999). In the Patagonian area it is found from the intertidal

zone up to 60 m (Boretto et al., 2019). The wide and flattened shells have an external sculpture with fine concentric lines, sometimes crossed by numerous radial groves (Boretto et al., 2014, Supplementary Figs. 4 and 5).

On the modern beach, we observed that articulated mollusk shells (not living) formed distinct zones that are always included between the ordinary berm (created by fair-weather waves) and a higher storm berm (created by sea storms in the area). To quantify the indicative meaning corresponding to these two morphological elements, we calculated the 2% exceedence wave runup level using different models implemented into the pywave-runup tool coded by Leaman et al. (2020).

The models require as input the beach slope (β), significant wave height (H_s) and period (T_p). We gathered the beach slope at six transects along the Camarones beach using the CoastSat.Slope toolbox (Vos et al., 2019, 2020). With this toolbox, we analyzed Landsat and Sentinel satellite data between 2000 and 2023, alongside with tides extracted from the FES2014 global tidal model (Lyard et al., 2021; Carrere et al., 2016). We calculated that β is 0.18 ± 0.02 (1σ). To calculate H_s and T_p we used the RADWave tool (Smith et al., 2020), which allows querying satellite altimetry data. We extracted a timeseries of wave data between 65°W and 61°W and 47°S to 43.5°S, in a period included between Jan 1st, 2000 and Jan 1st, 2023 (Fig. 2). For the same time frame, we queried the FES2014 model and extracted water levels at a 15-min interval. Coupling tidal and wave data via their UTC timestamps we gathered a database with 43102 wave conditions. For each condition, we selected a

beach slope sampled from a normal distribution created with the mean and standard deviation of β. We used the "ensemble" function of pywave-runup to run, for each wave height and period, eight runup models. At each calculated runup, we added (or subtracted) the corresponding water level derived from the FES2014 tidal model. The Jupyter notebooks used for this workflow are shared as part of the Supplementary Information.

3.3. Geochronological methods

Earlier authors applied the methods of Electron spin Resonance (ESR) and U-series to *A. antiqua* shell to obtain ages for the beach deposits in the Camarones region and were successful in differentiating beach ridges of different ages within the broader Patagonian region (e. g., Schellmann and Radtke, 2000; Pappalardo et al., 2015). However, both methods are recognized as having drawbacks and issues when applied to marine mollusk shell, with a primary concern being whether the shell behaves as an open or closed system (e.g., see discussions in Schwarcz, 1994; Hillaire-Marcel et al., 1996; Schellmann and Radtke, 2000; Schellmann et al., 2008), although recent method advancements in ESR appear to address this concern (Duval et al., 2020). Another common geochronological method used for the analysis of beach ridges is luminescence dating (see review by Lamothe, 2016); however, the composition of the beach ridges in Camarones and, in general, along the Patagonian coasts of Argentina (predominantly pebbles and cobbles
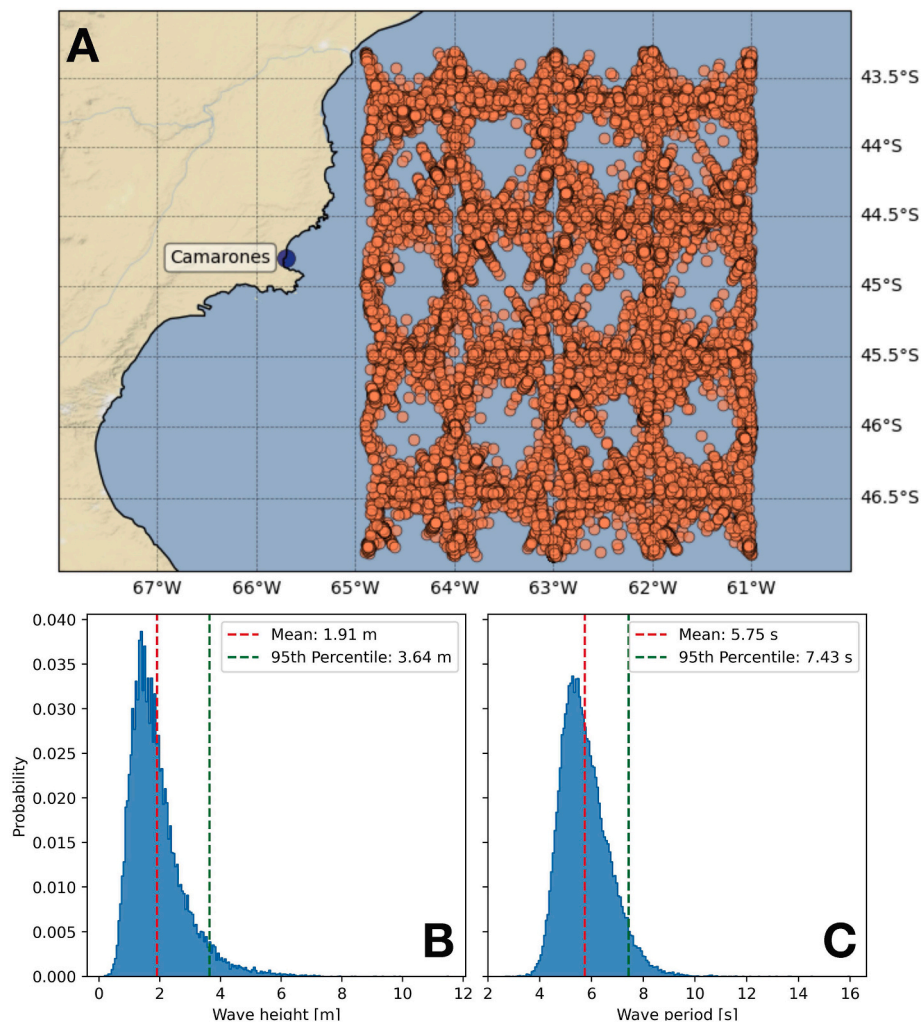

Fig. 2. A) Map of satellite altimetry tracks from which wave conditions offshore of Camarones were extracted (IMOS, 2023). B) and C) respectively, histograms of wave height and period.

with little to no sand) limits the application of that method with only one study showing reliable age estimates (Ribolini et al., 2011), albeit limited to the Early Holocene.

In our work we apply Amino Acid Racemization (AAR) and radiocarbon geochronological methods. AAR does not provide numerical ages (unless calibrated) but instead relative ages as indicated by the clustering of D/L values of amino acids and is useful in correlating deposits (see reviews of the method by Wehmiller, 1982; Wehmiller and Miller, 2000; Wehmiller, 2013b). AAR, like ESR and U-series, has been used successfully within Argentina to distinguish shells of MIS 5 age from earlier interglacials (see Gowan et al., 2021a, for review). Due to the uncertainties of each method, none are able to distinguish between MIS 5 substages (i.e., 5e, 5c, or 5a) with high certainty.

3.3.1. Amino acid geochronology

Articulated and disarticulated valves of *A. antiqua* were collected from beach ridge exposures at all sites except PE5E where only fragments of shell, tentatively identified as *A. antiqua*, were found on the surface. Between four and eight shells were selected from each Pleistocene site with consideration for their robust appearance, i.e., completeness of valve, a minimal indication of wearing, abrasion, or dissolution (the dated shells are shown in Supplementary Figs. 4 and 5).

Subsampling, sample preparation, and analysis were completed at the Amino Acid Geochronology Laboratory at Northern Arizona University. Shells were subsampled at the hinge-umbo region. Sample preparation and hydrolysis followed the methods established by Kaufman and Manley (1998). Samples were analyzed using an Agilent 1100 series RP-HPLC (reverse-phase–high-performance liquid chromatography) instrument. Interlaboratory comparisons (ILCs), homogenous powders of Pleistocene mollusk samples, were used as comparative standards (Wehmiller, 2013a).

The results of AAR analyses were subject to data screening to identify and reject D/L values that would compromise the integrity of the sample group. We used aspartic and glutamic acids D/L values to assess amino acid abundance and variance, and relative age. The preference for these amino acids is due to their high chromatographic resolution and individual characteristics (Goodfriend, 1991). Aspartic acid is present in very high concentrations in younger fossils, whereas glutamic acid has a stable kinetic behavior and is a reliable amino acid for discriminating age based on the extent of racemization. Serine was also used in data screening. Serine decomposes rapidly, and excessive amounts of serine in Pleistocene samples indicate contamination by modern amino acids (Kosnik and Kaufman, 2008).

Using these criteria, all results were accepted except for those from PE5E. The D/L values from this site were extremely inconsistent. Two samples were immediately rejected for serine abundance. The remaining D/L values exhibited high variation within their sample group and in comparison with the other field sites. Due to the inconsistency of the results, the unknown environmental history, and as we were initially uncertain of the genus of the shell fragments from which the samples were selected, we decided to reject all results from PE5E.

An additional valve of *A. antiqua* was collected from the modern beach berm of Camarones beach with paired analysis by radiocarbon (see below) to provide a comparison for the Pleistocene D/L values.

3.3.2. Radiocarbon

Two shells of the limpet *Nacella* sp., collected from a Holocene beach ridge, were selected for radiocarbon dating at the Beta Analytic laboratory using an in-house NEC accelerator mass spectrometers (AMS). Radiocarbon ages are reported as calibrated years (cal yr BP, 2σ) using CALIB software (version 8.2) and the MARINE20 curve (Heaton et al., 2020). A marine reservoir correction ($\Delta R = -174 \pm 132$) has been applied according to the closest available data for the study area using the Marine Reservoir Correction Database (Reimer and Reimer, 2001).

One disarticulated valve of *A. antiqua* was collected from the modern beach berm of Camarones beach and dated using radiocarbon paired with AAR (see above). This analysis was done to provide a numerical age constraint for the Holocene D/L values.
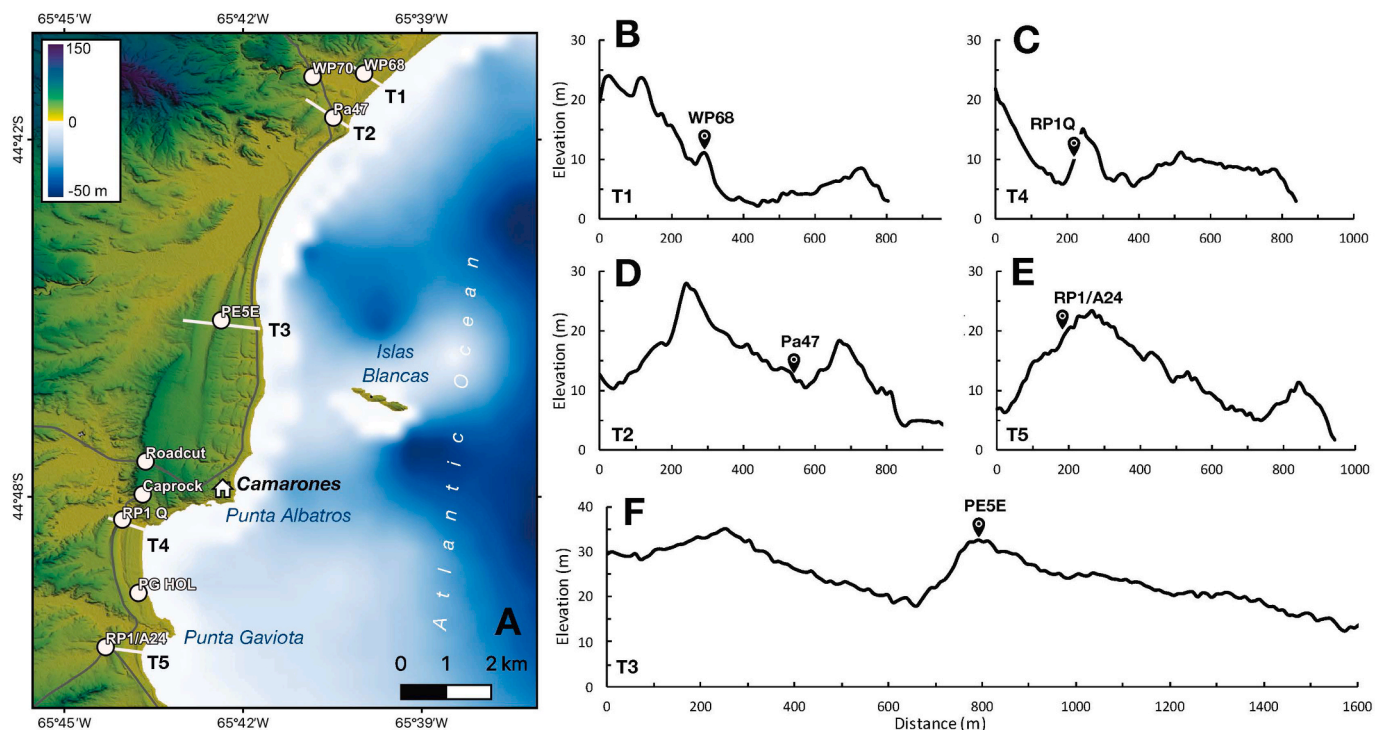

Fig. 3. Pliocene, Pleistocene and Holocene sites. A) Map of the study area, showing the location of the town of Camarones and the sites reported in this study. Topography from TanDEM-X Digital Elevation Model and bathymetry from GEBCO, 2023, B-F) Topographic transects and associated field sites described in the text.
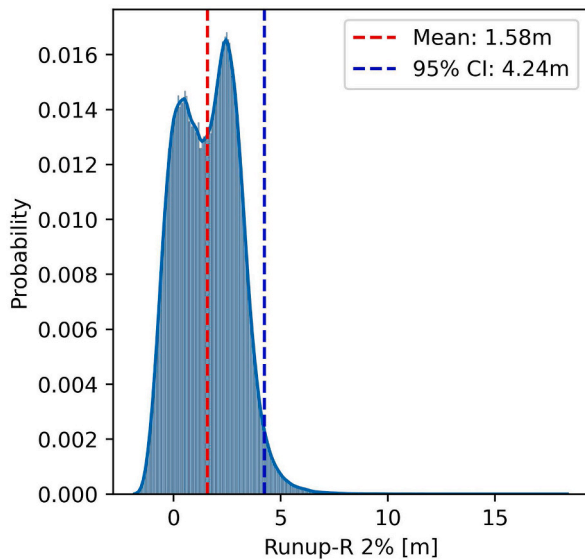
Fig. 4. Calculation of the indicative range for beach ridges at Camarones. Plot showing the probability distribution of 2% exceedance wave runup level plus water level from the FES2014 model calculated at Camarones for different runup models (Holman, 1986; Ruggiero et al., 2001; Stockdon et al., 2006; Nielsen, 2009; Senechal et al., 2011; Vousdoukas et al., 2012; Passarella et al., 2018; Beuzen et al., 2019).

4. Results

In the area of Camarones, we identified, sampled and surveyed seven sites (plus the two already reported in Rovere et al., 2020), that are described below and shown in Fig. 3.

4.1. Indicative meaning of beach ridges

Including the results of all runup models (Fig. 4 and Supplementary Fig. 6), we obtain that the 23-year average runup on the Camarones coast is 1.58 m, while the 95% extreme runup is 4.24 m. We use these two values as representative of the ordinary berm and the storm berm, respectively, which define respectively the lower and upper limits of the indicative range of beach ridges in the area. Using Equation (2) and Equation (3), we calculate that the RWL associated with the top of articulated shells in Camarones is 2.91 m and the associated IR is 2.66 m. We note that the RWL calculated with our approach is comparable to that obtained via the IMCalc tool (RWL = 2.3 m, IR = 0.6 m, Lorscheid and Rovere, 2019), which employs the Stockdon et al. (2006) model, with less accurate wave and tidal data, and a general beach slope. However, this model underestimates the IR and the final uncertainty on paleo RSL would be lower, but less accurate if we had applied the IMCalc method.

4.2. Holocene

The Holocene sea-level record surrounding Camarones is represented by 76 sea-level index points located between Cabo Raso (60 km North of Camarones) and Bahia Bustamante (80 km South of Camarones, Fig. 5 A), that were reported by several authors (Codignotto et al., 1992; Schellmann and Radtke, 2003, 2007, 2010; Ribolini et al., 2011; Zanchetta et al., 2012; Bini et al., 2018). These datapoints are here reviewed (see Supplementary Information for details) following the HOLSEA standards (Khan et al., 2019b). In general, the Holocene data in this area extend back to 8 ka BP, with a highstand reaching up to 6–8 m above present sea level between 4 and 6 ka (Fig. 5 B). In 2019, we collected two shells of the limpet *Nacella* sp. from a Holocene beach ridge close to Punta Gaviota (site PG Hol). The shells were collected from the upper
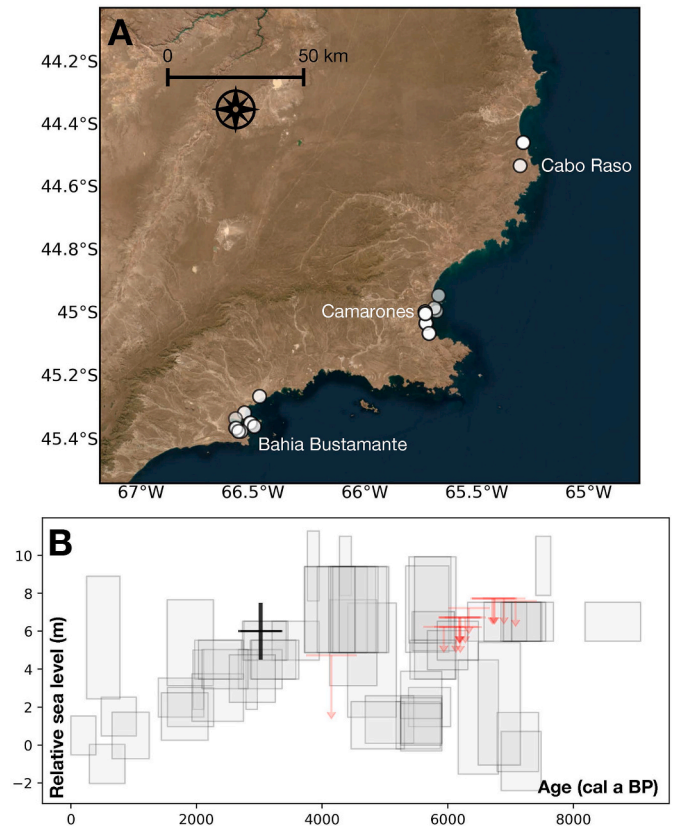

Fig. 5. Holocene sea-level index points. A) map of Holocene sea-level index points in the broader area around Camarones (white dots). B) Relative sea level vs Age plot of the RSL index points shown in A). Red arrows show terrestrial limiting points, which indicate that sea level was below the horizontal red bar. The black cross indicates data gathered in this work, while the gray boxes indicate data from literature. Elevation error bars are 1σ, while age error bars are 2σ.

part of the ridge (elevation: 8.7 ± 0.22 m, 1σ), and represent the highest occurrence of shells (in terms of elevation above sea level), located few decimeters from the top surface of the ridge. Using the same indicative meaning adopted for Pleistocene ridges in the area, we calculate that the paleo RSL when this ridge was formed was 6 ± 1.5 m (1σ). Radiocarbon ages (see Supplementary Information for details) indicate an age of this beach ridge ranging from 2663 to 3369 cal yr BP (2σ range).

4.3. Pleistocene highstands

Within the study area, five Pleistocene beach ridges were resurveyed and sampled during our fieldwork. These deposits have been previously described and dated by several authors (Schellmann, 1998; Schellmann and Radtke, 2000; Pappalardo et al., 2015). In our work, we have retained the site names used in the studies cited above, unless specified in the text below. From north to south, the sites related to the Pleistocene highstands in the area are: WP68, WP70, Pa47, RP1 Quarry, and RP1/A24 (Fig. 3 A).

4.3.1. WP68

The first beach ridge we surveyed is located about 40 km North of Camarones (Fig. 3 A). We maintained the site name of Pappalardo et al. (2015), who describe this site as composed by a ridge *"displaying poor morphological evidence but good lateral continuity towards NE"*. Such morphology is evident from digital elevation models (Fig. 3 B). Pappalardo et al. (2015) dated an articulated specimen of *A. antiqua* with U-series and obtained an age of 131 ± 1.1 ka (2σ range). In our survey, we collected four shells of the same species (none articulated) from the

surface of the ridge for AAR analysis (Supplementary Fig. 5), which reaches a maximum elevation of 12.2 ± 0.23 m (1σ). This altitude is roughly the midpoint between ridge-top elevations recorded at sites Pa47 (11.3 ± 0.2 m) and RP1 Quarry (14 ± 0.2 m), described below.

4.3.2. WP70

About 1.2 km West of WP68 (Fig. 3 A), we surveyed a marine deposit overlying a shore platform carved on the bedrock, previously described by Pappalardo et al. (2015). These authors dated an articulated *A. antiqua* shell collected from the marine deposit, which they described as sandy with sorted gravels and abundant marine shells. U-series analysis gave an age of 127 ± 1.2 ka (2σ, sample WP70B). In 2022, we surveyed the contact between the bedrock platform and the overlying deposit to an elevation of 13 ± 0.22 m (1σ). We did not find any shell to sample within this deposit. However, ~173 m SW of the bedrock platform, we found a small quarry with a good lateral continuity where we sampled a layer containing *A. antiqua* shells (4 samples, no articulated shells, Supplementary Fig. 4) at an elevation of 10.3 ± 0.22 m (1σ). We do not use this site in our paleo RSL calculations, as it is located within a former embayment, which could have been affected by stream erosion and re-deposition after the emplacement of the marine deposits. However, we note that both the bedrock platform and the ridge are found at elevations consistent with those of RP1 Quarry and the Pa47 ridge, described below.

4.3.3. Pa47

About 1.4 km South of WP70 (and ~11 km North of Camarones town, Fig. 3 A), we identified a beach ridge that abuts directly onto higher terrains (Fig. 3 D). Quarrying activities in this area have exposed a small outcrop of about 1.15 m in height. This outcrop is divided into two sedimentary units composed mainly of pebbles with a fining upward sequence. The upper part of the second unit shows soil development, and in its lower part includes shells of *A. antiqua*, with few articulated specimens. Within this unit, we also identify specimens of the mollusk *Tegula atra*, which is used as a Pleistocene biostratigraphical tool in the

marine Quaternary of Argentina (Aguirre et al., 2013). The site name is derived from Schellmann and Radtke (2000), who collected shells from two layers at this site, one from the upper unit (Pa47c) and one from a lower unit (Pa47a). Several ESR and U-Series dates yielded average ages 102 ± 10 ka and 129 ± 16 ka for the upper and lower unit, respectively. During the 2022 campaign, we collected four disarticulated valves of *A. antiqua* from the upper unit (Supplementary Fig. 4). The top of the beach ridge is 11.3 ± 0.2 m (1σ), and the articulated shells are located 28 cm below this point. This corresponds to a paleo RSL of 8.4 ± 1.5 m (1σ).

4.3.4. RP1 quarry

About 14 km South of Pa47 (and ~2 km south of the town of Camarones, Fig. 3 A), we re-surveyed a beach ridge along the *Ruta Provincial* 1. This site has the morphology of a single, isolated ridge (Fig. 3 C). The landward side of the beach ridge has been quarried (likely by roadworks), exposing the complete ridge stratigraphy in a clean vertical section on average ~4.5 m high (Fig. 6A and B). Within this section, Pappalardo et al. (2015) identify two units of sorted coarse sands and gravels with abundant marine fauna separated by a centimeters thick layer of silty clay with gravel throughout. This section was revisited in the 2019 field campaign. The presence of two units (U1 and U2 in Fig. 6 D) was confirmed. The boundary between them is represented by discontinuous, lense-shaped, fine materials, with traces of oxidation pervading the lower unit. The lower unit (U1) is sandy, with scattered gravels and fragmented shells. Coarseness and the abundance of shells increase upwards, where the deposit becomes clast-supported. At this transition, articulated shells of *A. antiqua*, not in living position, cluster. A small barnacle colony (12 individuals, Fig. 6 E) was found in an upright position anchored to an *A. antiqua* shell at an elevation of 10.3 ± 0.22 m (1σ). The overlying unit (U2) is similar to the lower one but with whole and articulated valves of *A. antiqua* clustering at the bottom (Fig. 6 C). On the whole, the sequence can be interpreted as two beach ridge deposition phases separated by an ephemeral water body in an interridge swale deposit, as previously described by Pappalardo et al.
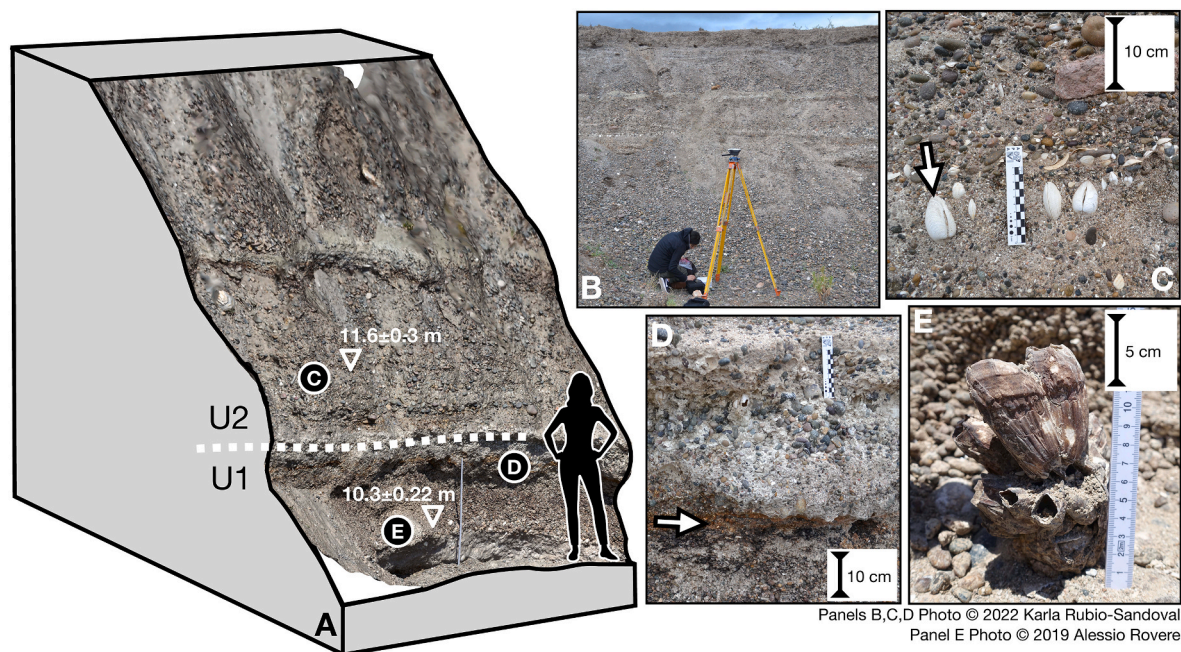

Panels B,C,D Photo © 2022 Karla Rubio-Sandoval
Panel E Photo © 2019 Alessio Rovere

Fig. 6. RP1 Quarry site. A) 3D view of the RP1 Quarry outcrop, reconstructed via overlapping field photos processed with Structure-From-Motion Multi View Stereo techniques. Downward pointing triangles with values show GNSS data collected at this site, while circled text refers to other panels in the figure. U1 and U2 refer to the two units identified in this outcrop, described in the main text. B) View of the main face of the RP1 Quarry outcrop. C) Uppermost articulated shells (arrow) within the beach ridge (U2), see location and elevation in panel A. D) Oxydised silty clay layer (arrow) with gravels already identified by Pappalardo et al. (2015), see location in panel A. E) Colony of barnacles (*Balanus* sp.) in living position, see location and elevation in panel A.

(2015). These authors sampled a specimen of *A. antiqua* from the uppermost layer and employed U-series to date it to 92 ± 0.6 ka (2σ, sample WP92A(3)). Within the layer dated by Pappalardo et al. (2015), we surveyed the highest occurrence of articulated shells at different positions along the exposed section (~30 m across) without recording significant height changes. Overall, averaging the elevation of 5 points, we calculate that the elevation of this layer is 11.6 ± 0.3 m (1σ), corresponding to a paleo RSL of 8.9 ± 1.5 m (1σ). At this site, we collected 7 specimens of *A. antiqua* for AAR analysis, two of them articulated (Supplementary Fig. 4).

4.3.5. RP1/A24

South of the town of Camarones, about 1.5 km onshore *Punta Gaviota* (Fig. 3 A) and close to the intersection between *Ruta Provincial* 1 *and Ruta Provincial* A24, we surveyed both in 2014 and in 2019 a site that we hereby call "RP1/A24" (Fig. 7A–C). A road cut on the backshore slope of a beach ridge exposes part of the stratigraphy of this feature, formed by rounded pebbles embedded in a sandy matrix. Within the deposit, a layer containing a cluster of articulated *A. antiqua* mollusk shells is present. (Fig. 3E). The coastal deposit was sampled and dated at the same site with both U-series and ESR by Schellmann (1998), as further described in Schellmann and Radtke (2000) (Sample Pa35). These authors initially attributed this deposit to MIS 9, as it yielded ESR ages scattered between 342 ± 29 ka and 383 ± 28 ka. An U-series age on the same shells yielded an age of 228 ± 15 ka, but Schellmann and Radtke (2000) state that it "*seem[s] to be too young by a factor of up to 2*", hence opening up the possibility that this shell dates to MIS 11. It is worth noting that Schellmann and Radtke (2000), discussing this site, surmise that ESR ages older than 300 ka are at the upper limit of the ESR dating technique, therefore they might be less reliable. One sample, labelled WP97(1), from the same deposit was dated with U-series by Pappalardo et al. (2015), yielding an age of 414 ± 16 ka (2σ). We collected eight articulated *A. antiqua* shells at this site for AAR analysis (Supplementary
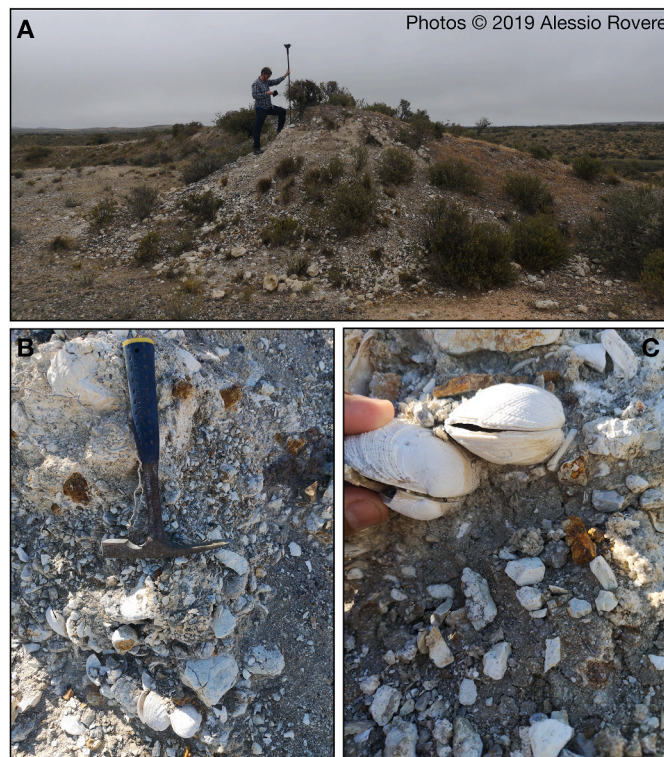

Fig. 7. RP1/A24 site. A) overview of the beach ridge, with co-author E.J. Gowan measuring the highest occurrence of articulated *A. antiqua* mollusk shells. B) and C) details of the beach ridge where articulated *A. antiqua* mollusk shells occur.

Fig. 5). We surveyed the elevation of the top of this deposit four times, three in 2014 and one in 2019, obtaining an average elevation of 17.2 ± 0.2 m (1σ), corresponding to a paleo RSL of 14.5 ± 1.5 m (1σ).

4.4. Pliocene highstand

Rovere et al. (2020) report two outcrops, that were named "Roadcut" and "Caprock" south of the town of Camarones (Fig. 3 A). Both are transgressive sequences on top of an uplifted shore platform. In both outcrops there is a unit described as a conglomerate with bivalve shells that were reported as mostly intact and sometimes with articulated valves (Rovere et al., 2020). Strontium isotope stratigraphy dating on oyster shells assessed that this unit is Early Pliocene in age (4.69–5.23 Ma, 2σ). The elevation of this unit was measured at 36.2 ± 0.9 m (1σ) above mean sea level, and paleo RSL was reconstructed at 36.2 ± 2.7 m (1σ) above present sea level, as the unit was interpreted as indicative of a foreshore (intertidal) environment. About 4 km North of the Roadcut outcrop, we surveyed a beach ridge prominent within the landscape (PE5E, Fig. 3 A and F) that sits at elevation similar to those of the "Roadcut" and "Caprock". As the beach ridge did not have an exposed outcrop, we measured its top giving an elevation of 31.7 ± 0.2 m (1σ). From the ridge surface we collected broken, rounded fragments tentatively identified as remains of *A. antiqua* shells, which appear highly reworked (Supplementary Fig. 5).

4.5. AAR results

In this work, we compare the results of previous dating (reported in the site descriptions above) with AAR on the same shell species with the aim of evaluating the consistency of the chronological attribution done by previous authors in this area. All our analytical results are reported in the Supplementary Information annexed to this paper. All dated shells are shown on Supplementary Figs. 4 and 5. One *A. antiqua* shell collected from the modern beach ridge south of Camarones and seaward of the field site RP1, yielded a radiocarbon age of 698 ± 137 cal a BP (2σ).

Shells sampled from Pleistocene deposits have much higher D/L glutamic - aspartic acids ratios than the one sampled within the Holocene beach ridge (Fig. 8). The aspartic and glutamic acids D/L values from the Pleistocene beach ridges form two distinct clusters indicating at least two different depositional periods (Fig. 8, Supplementary Fig. 7). Due to the close proximity of the sites and a regional mean annual temperature of 13 °C, the effective diagentic temperature is expected to be consistent across all sites and we can discount temperature differences as a driver for the different groupings. Most sites are grouped within the younger cluster, whereas the older cluster is formed predominantly by shells collected from RP1/A24. These groupings are broadly consistent with the ESR and U-series ages reported by earlier authors (Schellmann and Radtke, 2000; Pappalardo et al., 2015).

AAR ratios from the four shells sampled at Pa47 are split between the two groups described above. The geomorphological evidence, elevation of articulated shells, and former ESR and U-series dating at site Pa47 align with those reported at RP1 Quarry, WP68 and WP70. Therefore, we suspect that Pa47 includes older reworked shells, possibly washed down from higher terrains (Fig. 3 D). Schellmann and Radtke (2000) and Pappalardo et al. (2015) identified an unconformity at this site, with the latter authors attributing the deposit above the unconformity to storm activity and reworking of earlier deposits. It is reasonable then to interpret the higher D/L values as reflecting the redeposition of shells from an earlier interglacial of similar, if not the same age, as RP1/A24.

The two AAR clusters identified in this study are correlated, by the U-series and ESR ages of previous authors (Fig. 8), to MIS 5 (likely MIS 5e) and either MIS 9 or MIS 11 Supplementary Fig. 7).

5. Discussion

In this work, we use both previously published and original data to
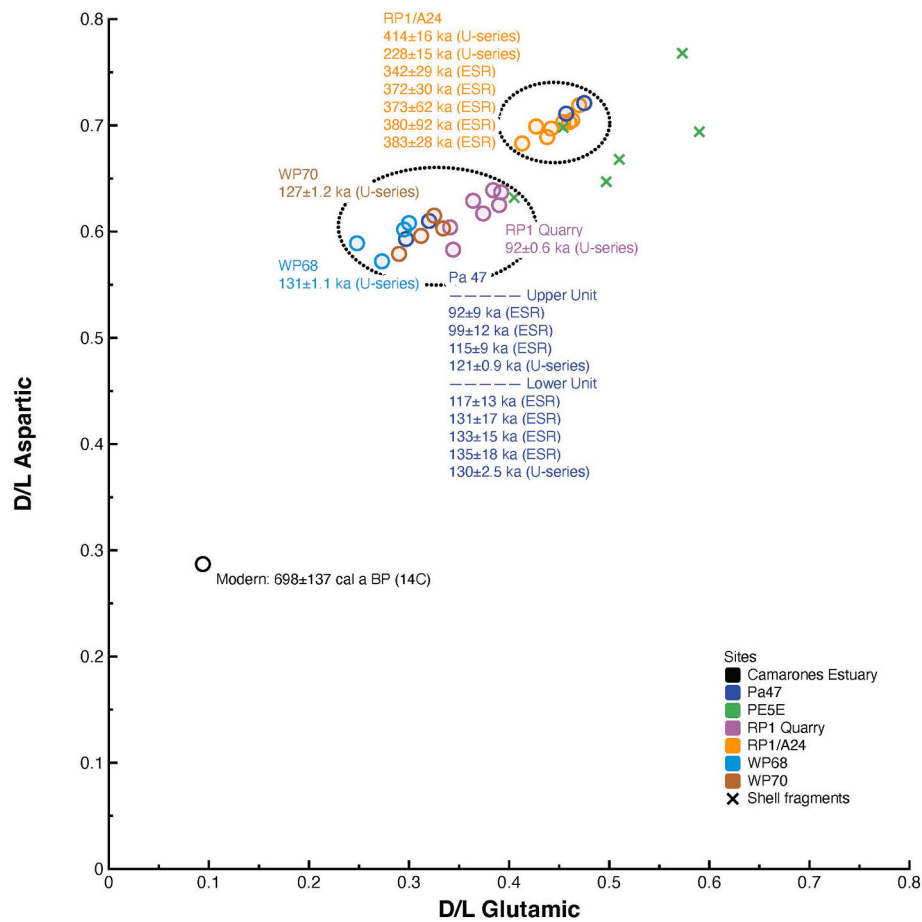
Fig. 8. AAR, U-series and ESR ages available in the Camarones area. Results of Amino Acid Racemization (aspartic acid and glutamic acid D/L values) on specimens of *A. antiqua* collected from beach ridges in the Camarones area. Colors identify different sites described in the text, and the colored text reports the results of radiometric dating on shells from the same beach ridges (age uncertainty assumed as 2σ, data from Schellmann and Radtke, 2000; Pappalardo et al., 2015). The different symbols identify if the specimen was an integer valve (circle) or a shell fragment (cross, rejected). The dotted ellipses identify the two age groups discussed in the main text.

investigate past sea-level highstands in the Camarones area. As highlighted by previous authors, within a short geographic distance around the town of Camarones, the imprint left by sea level during several past highstands has been left on the coastal landscape (Supplementary Fig. 8). As such, this area has preserved an exceptional record of sea-level changes through time.

5.1. Relative sea level, GIA and post-depositional uplift

Data on the Holocene beach ridges show a RSL peak between ~4 and 7 ka, when sea level reached up to 4–8 m above present-day (Fig. 5). These observations are in broad agreement with Glacial Isostatic Adjustment (GIA) models (Supplementary Fig. 9), which predict a GIA-induced RSL peak of comparable magnitude and timing (Fig. 9 A). The Holocene provides important insight into how strandplains of beach ridges at this location (and arguably over the Patagonian coast) develop over an interglacial and are preserved during successive interglacial periods.

The highest ridges within a given interglacial are those deposited during the RSL highstand, which at this location is dictated by GIA processes including ocean siphoning, continental levering, and rotational feedbacks (Mitrovica and Milne, 2002; Peltier, 2002; Argus et al., 2014; Peltier et al., 2015). The influence of syphoning, and the rotational term means that the sea level highstand in Camarones and elsewhere in Patagonia is sensitive to the history of Northern Hemisphere ice sheets. So far, there is no strong evidence of the Patagonian ice sheet

control on Holocene sea level in this area. Rostami et al. (2000) suggest that due to the small ice sheet thickness (ca. 400 m), there is no significant effect on the RSL along the coast of Argentina. However, Björck et al. (2021) state that the Patagonia ice cap may contribute to the GIA signal in the southern part of Patagonia.

As the GIA-driven sea-level regression evolves, it may leave behind a set of regressive ridges, that may be eroded away if RSL reaches a similar elevation during a successive highstand. It follows from this reasoning that the ridges we surveyed represent the peak relative sea level associated with each period. In fact, Rostami et al. (2000) highlight the absence of paleo shorelines deposited during MIS 7 in the Patagonian coastline of Argentina, suggesting a reoccupation of these deposits during the subsequent MIS 5 transgressive event, when the sea level rose to a higher elevation.

Our survey results at RP1 Quarry (RSL = 8.9 ± 1.5 m, 1σ) and Pa47 (RSL = 8.4 ± 1.5 m, 1σ) represent, on average, a paleo RSL of 8.7 ± 2.1 m (1σ). AAR clusters these sites as of similar age to WP68 and WP70 (Fig. 8), which, albeit less indicative in terms of paleo RSL, are consistent in elevation. The radiometric ages of these sites are predominantly skewed towards the early part of MIS 5e, in agreement with both the evolution model proposed above and models predicting a GIA driven sea-level highstand of similar magnitude to the Holocene one at ~128 ka (Fig. 9B and C). GIA models predict that a shoreline deposited 128 ka ago would have formed 5.8 ± 3.9 m (1σ) higher due to GIA alone, yielding a GIA-corrected relative sea level of 2.9 ± 4.4 m (1σ) above present.
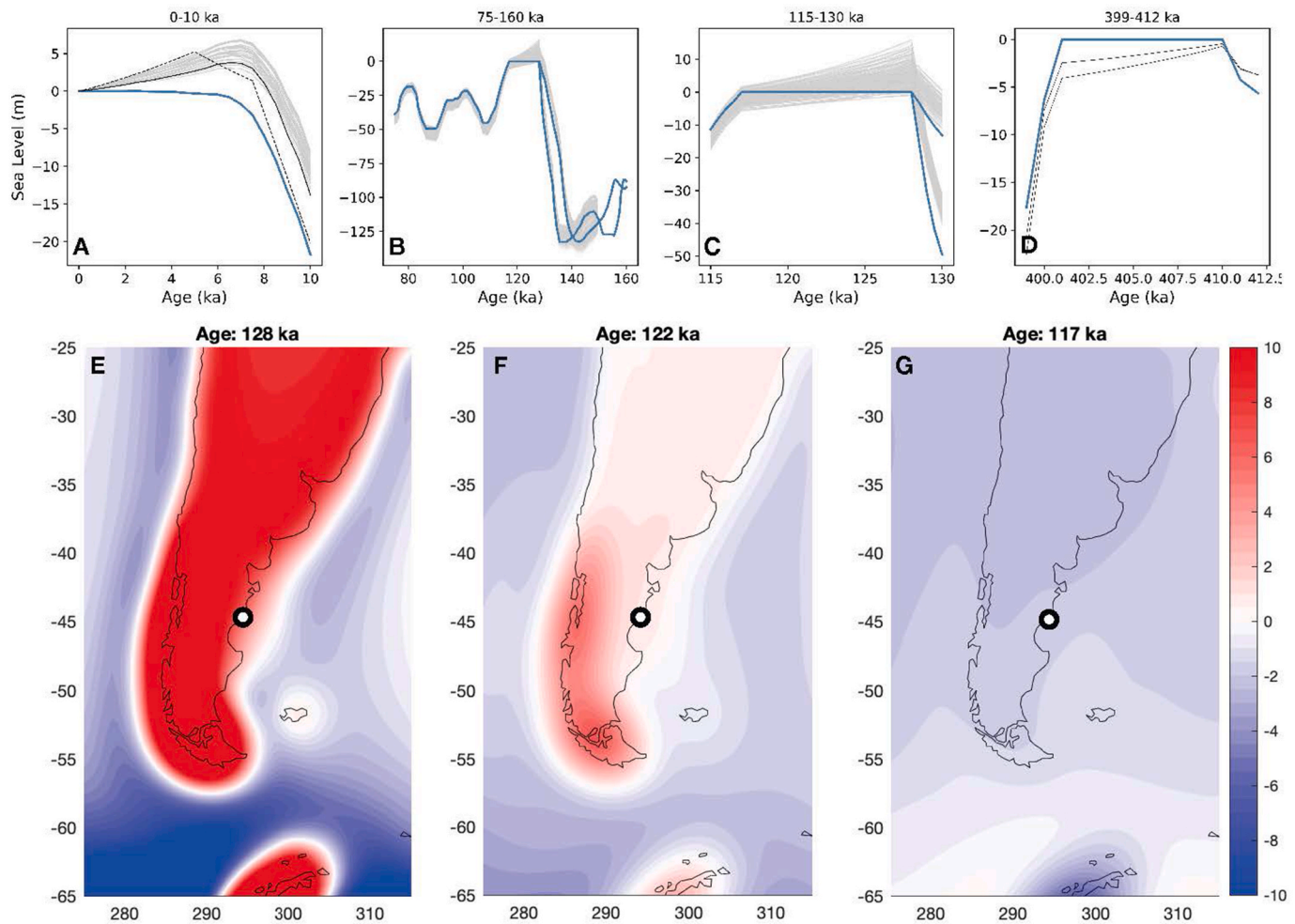
Fig. 9. Published GIA models in the area of Camarones. A) Holocene (gray lines, GIA from Dyer et al., 2021, dashed line from Gowan et al., 2021b, solid black line from Peltier et al., 2015), B) MIS 5 (from Dyer et al., 2021), C) MIS 5e (from Dyer et al., 2021), D) MIS 11c (from Raymo and Mitrovica, 2012). The blue line in A-D represents GMSL. In B-C-D, the sea-level caps at 0 m as per model input, to show only the background GIA response. E, F and G, spatial pattern of mean GIA changes throughout MIS 5e across the broader South American region. The white dot shows the location of Camarones.

From the work on early Pliocene shorelines in the region (Hollyday et al., 2023), it appears that Dynamic Topography (DT) has played a major role in uplifting shorelines through time at this location. The mean DT change since 1 Ma from the four best-fitting DT models of Hollyday et al. (2023) predicts an uplift of 40.1 ± 4.5 m/Myr (1σ, equivalent to 0.0401 ± 0.0045 mm/yr). This value may seem at odds with the elevation of the early Pliocene shoreline at 36.2 ± 2.7 m, which has been used to calibrate the geodynamic model since it would imply that this shoreline was uplifted by approximately 200 m.

There are two reasons for this discrepancy. First, while the models of Hollyday et al. (2023) predict approximately linear DT change over 1 Myrs in this region, deformation is not linear over longer timespans. Second, Hollyday et al. (2023) explore uplift rates around the data location according to the spatial resolution of the seismic tomography model that determines the pattern of convection. Therefore, their estimate does not exactly align with the location of the shoreline.

Applying the above-mentioned rate to an age of 128 kyr yields 5.1 ± 0.6 m of uplift. Austermann et al. (2017) use similar but uncalibrated geodynamic models and predict a similar but much more uncertain uplift of 3.6 ± 5.9 m. Assuming the rate of Hollyday et al. (2023) yields an uplift corrected sea level estimate of −2.2 ± 4.4 m for MIS 5e for Camarones. To infer GMSL, this value further needs to account for the fingerprint signal of excess melt during MIS 5e (Hay et al., 2014). Melting from the West Antarctic ice sheet would cause sea level to rise

less in Patagonia compared to other sites, which may explain this relatively low value. However, additional GIA modeling is required to investigate whether this value is reconcilable with sea level observations from other locations or whether the uplift rate requires revision.

The age attribution of this site is not straightforward. U-series places the ridge firmly within MIS 11 but the uncertainty of the ESR ages is suggestive of either an MIS 9 or 11 age. However, the ages suggest this site to be at the upper limit of the dating technique (Schellmann and Radtke, 2000). The AAR results are more indicative of MIS 9 (see below discussion).

There are no models available to correct a MIS 9 (~330 ka) shoreline for GIA at this location. However, if the same uplift rate as discussed above is applied here assuming an MIS 9 age it would result in an uplift-corrected sea level of 1.3 ± 2.1 m (1σ). If the GIA signal is small, this sea level inference would be in line with studies surmising that sea level during MIS 9 was close to present-day (Murray-Wallace, 2002).

For MIS 11, GIA models published by Raymo and Mitrovica (2012), predict that RSL was 0.6 ± 0.2 m (1σ) below GMSL at ~410 ka (Fig. 9 D). Additional melt during this time period might have changed the timing of peak sea level, which affects the GIA correction. We remark that the smaller uncertainty of this prediction compared to that reported for MIS 5e is due to the fact that the MIS 11 predictions employ fewer mantle viscosity profiles and ice sheet configurations than those employed for MIS 5e (Dyer et al., 2021). Using the rates from DT models

to correct this shoreline for vertical land motion leads to a GIA and uplift corrected sea level of -1.3 ± 2.4 m (1σ). While this still requires a correction for the fingerprint signal of excess melt it does appear low compared to existing estimates of GMSL during MIS 11 (Chen et al., 2014; Raymo and Mitrovica, 2012), which might indicate an overestimation of uplift driven by DT, an incorrect GIA correction, or an incorrect attribution to MIS 11, as discussed above.

The highest (36.2 ± 0.9 m, 1σ) and oldest (4.69–5.23 Ma, 2σ) shoreline in the area was reported by Rovere et al. (2020). Here, we tentatively attribute the large ridge we surveyed to the North of Camarones (where sample PE5E has been collected) to the same Pliocene highstand. Analysing this line of evidence in conjunction with other two sites of similar age along the Patagonian coast (Del Río et al., 2013). Hollyday et al. (2023) surmised that, once corrected for GIA and DT, these sites would indicate a GMSL of 17.5 ± 6.4 m (1σ).

5.2. Geochronology

A. antiqua shells are relatively large, thick, and robust (Supplementary Figs. 4 and 5) and for these reasons the inner portion of the shell structure is more likely to maintain its integrity through time, which has made it a preferred choice for geochronological methods in this and earlier studies. However, because of the uncertainties regarding the shell structure, it is important to apply multiple geochronological methods to *A. antiqua* in the absence of other complimentary methods (i. e., luminescence dating of sediments). The coherence of results within the same unit, between and within methods, reduces overall uncertainty that may result from the use of a single method.

In our results, there are some inconsistencies between the AAR D/L values and the radiometric ages. Sites WP68 and WP70, which have the highest U-series ages (within MIS 5, ~131 ka and ~127 ka, respectively), returned consistently (relatively) lower D/L values than site RP1, which provided the youngest U-series age (~92 ka, Fig. 8). Although the mean D/L values of the seven shells collected from RP1 are consistent within two standard deviations with the other MIS 5 ridges (WP68, WP70), glutamic D/L values from RP1 tend to plot higher in comparison with other sites and indicate a potentially older age. The U-series age was derived from a shell collected above the salitral lens identified by Pappalardo et al. (2015). The AAR result (ID 22680) of the shell we collected from the same unit is consistent within one standard deviation to the D/L values from WP68 and WP70. The remainder of the shells collected at RP1 for AAR analysis are from the lower unit and are stratigraphically consistent with earlier deposition. If we are to consider RP1 to have been developed completely within MIS 5, the AAR results would imply that the lower unit exposed at RP1 formed early within MIS 5e and that the unit above the salitral lens and the other MIS 5e exposures around Camarones are from a later point within that interglacial.

Two of the ESR ages (Pa47) and the U-series age mentioned above (RP1 Quarry), suggest the presence of shells dating to MIS 5a and MIS 5c within the ridges that we attribute to MIS 5e Fig. 8. The 'young' ESR ages are derived from shells taken from the upper unit at Pa 47. Our AAR results for these two sites correlate instead with MIS 5e. Given the consistency of the AAR data with the other ESR and U-series ages at Pa 47 and ridges WP70, WP68, and RP1/A24 (i.e., the AAR D/L values fit within their respective clusters), one of two hypotheses is possible.

First, it is possible that the anomalously young U-series and ESR ages are outliers, underestimating the actual age of the shells. Under this assumption, their true age would be correlated to MIS 5e. In this context, it is worth mentioning that all three geochronological methods (ESR, U-series, and AAR) used to determine the age of the beach ridges at Camarones suffer from uncertainties associated with the nature of the shell structure and whether it behaves as an open or closed system. A closed system increases the likelihood that whatever variable the method measures, whether it is a trapped charge, uranium-thorium, or amino acids, is endogenous to the shell and has not been altered by external environmental factors after death and during diagenesis. For

this reason, all these methods employ sample collection and preparation steps to minimize both the inclusion of exogenous materials/isotopes in the sample and any physical or chemical alteration or diagenesis that may influence the result, also accounting for any intra-shell variability. However, the integrity of the organic matrix of any shell and its rate of decay varies between mollusc species (Labonne and Hillaire-Marcel, 2000; Jedoui et al., 2003). The only way to accurately assess these variables in any species is through experimental studies designed for that purpose. This work has yet to be done for *A. antiqua*.

A second hypothesis is that the younger shells are the result of transport, in this case by coastal processes, during MIS 5a and/or MIS 5c. If we accept the upper boundary possible for preferred peak GMSL values during MIS 5a and 5c of $+1$ m and $+2$ m, respectively, as suggested by Creveling et al. (2017), it is possible that these substages peaked close to the MIS 5e shoreline and that shells were transported during the most extreme storms to the height of the earlier shoreline. Our results (Supplementary Figure 6 I) show that his might be possible, as the 95% upper CI of wave runup in the area is 4.2 m. North of Camarones, in the Río de la Plata estuary, Rojas and Martínez (2016) reported higher-than-present littoral deposits of MIS 5a age. These deposits support the possibility that elevated MIS 5a aged deposits also exist in Camarones.

Another inconsistency in the geochronology is for the ridge surveyed at the RP1/A24 site, where RSL is estimated at 14.5 ± 1.5 m (1σ). The U-series age of 414 ± 16 ka is consistent with a MIS 11 age (Fig. 8), whereas the ESR ages can be interpreted as indicative of either MIS 9 or MIS 11, and are at the limit of the dating technique (Schellmann and Radtke, 2000). The consistency of amino acid kinetic pathways indicates a preference for an MIS 9 age, i.e., the D/L values from the RP1/A24 fossils are lower than what would be expected for an MIS 11 fossil given the regional temperature (CMAT 13 °C) and D/L values of the apparent MIS 5-aged fossils.

6. Conclusions

In this work, we presented new data on a set of beach ridges of different ages in the area of Camarones along the coasts of Patagonia, Argentina. Although beach ridges are one of the most common landforms across the entire Patagonia coast, their use as reliable sea level indicator poses a challenge due to their genesis, that is more related to wave intensity than directly to sea-level. In this work, we outline a new self-consistent and repeatable methodology to calculate their indicative meaning, i.e., to quantify the modern elevation of a fossil beach ridge with respect to paleo sea-level. We build upon modern wave data and a suite of wave runup models to estimate their upper and lower limits. We surmise that this approach, using 23 years of wave data, is more robust than measuring the modern analogue (i.e., the ordinary and storm berms along the modern coast) at a single time, as in the case of beach ridges these might be ephemeral and dependent on recent storm activity rather than on long-term wave regimes. We highlight that there might be other issues to take into account, which we do not consider here. For example, the indicative meaning obtained with this method should be corrected for the increased or decreased water levels related to storm surge under different climate conditions (Scussolini et al., 2023).

In any case, the method to estimate the indicative meaning adopted here appears more reliable (as it is based on local wave and beach topography data) than the one proposed by Lorscheid and Rovere (2019), who use global wave atlases and global beach slope values. For this reason, we surmise that an update of the recent work of Gowan et al. (2021a), that was carried out revising the indicative ranges of Pleistocene beach ridges along the Patagonian coast done using the methodology proposed by Lorscheid and Rovere (2019) may be granted.

Additionally, we provided new AAR data by analyzing *A. antiqua* shells, our results complement ESR and U-series ages obtained by previous works. Our chronostratigraphic approach allowed to identify four interglacial beach ridge systems from the present-day coastline up to 2

km inland. The first (lowermost and seaward) ridge formed under a paleo RSL of 6 ± 1.5 m and is correlated with the late Holocene. The second (paleo RSL 8.7 ± 2.1 m) is correlated to MIS 5e. The third Pleistocene ridge system could be associated with either MIS 9 or MIS 11 (paleo RSL 14.5 ± 1.5 m), and the fourth (which was already reported by Rovere et al., 2020) is associated with the Early Pliocene (paleo RSL 36.2 ± 2.7 m).

There are still some discrepancies between ages of shells within the same beach ridge. For example, some radiometric ages also seem to suggest the inclusion in the MIS 5e beach ridge of MIS 5a and 5c shells, which may be due to problems with U-series and ESR ages, or caused by coastal transport during MIS 5a and MIS 5c. Due to the limitation of the dating techniques, it also is difficult to disentangle MIS 11 from MIS 9 at Camarones. However, AAR results suggest that it is likely that there is an imprint of MIS 9 sea level at Camarones. This would represent one of the few relative sea-level index points for this highstand globally.

Our research highlights that there is a need of refined GIA predictions to back-calculate GMSL from the observed proxy data in this area. For MIS 5e, a refinement of the broad span of GIA predictions, accounting for the spatially varying sea level signature of excess melt, and further corrections for vertical land motions are needed before obtaining a reliable global mean sea level estimate.

Finally, we hypothesize that further melt during the LIG may have affected when peak sea level is attained at this location and therefore it may also affect the GIA correction for this site. One strategy to reduce uncertainties in this regard may be to select the mantle viscosity profiles providing a better match with Holocene sea-level index points, and then investigating the corresponding predictions for MIS 5e and MIS 11. However, observations during different interglacials may be sensitive to different parts of the mantle depending on the melt history and melt source. Also, DT rates may need refinement. Those derived from published models (which were calibrated over the coasts of Patagonia by Hollyday et al., 2023) may overestimate the amount of uplift.

7. Funding

Author contribution statement

Karla Rubio-Sandoval and Alessio Rovere: Conceptualizazion, Writing-original draft. Marta Pappalardo and Deirdre Ryan and Sebastian Richiano and Evan J. Gowan: Writing - Review and editing. Alessio Rovere and Marta Pappalardo and Karla Rubio Sandoval and Evan J. Gowan and Sebastian Richiano and Luciana M. Giachetti: Investigation (field data and related analyses). Darrell Kaufman and Jordon Bright and Deirdre Ryan: Investigation (AAR data and related analyses). Jacqueline Austermann and Andrew Hollyday: Investigation (DT and GIA models).

Declaration of competing interest

The authors declare that they have no known competing financial interests or personal relationships that could have appeared to influence the work reported in this paper.

Acknowledgments

Appendix A. Supplementary data

Supplementary data to this article can be found online at https://doi.org/10.1016/j.quascirev.2024.108999.

Data availability

The data used in this paper are available on Zenodo (https://doi.org/10.5281/zenodo.10427736) with a CC BY 4.0 license. Supplementary figures are available for download from Elsevier and are attached to the preprint of this paper published in EarthArXIV (https://doi.org/10.31223/X5X11H).

References

Aguirre, M.L., Richiano, S., Donato, M., Farinati, E.A., 2013. Tegula atra (lesson, 1830) (Mollusca, gastropoda) in the marine quaternary of patagonia (Argentina, SW atlantic): biostratigraphical tool and palaeoclimatepalaeoceanographical signal. Quat. Int. 305, 163–187.

Argus, D.F., Peltier, W., Drummond, R., Moore, A.W., 2014. The Antarctica component of postglacial rebound model ICE-6G_C (VM5a) based on GPS positioning, exposure age dating of ice thicknesses, and relative sea level histories. Geophys. J. Int. 198 (1), 537–563.

Austermann, J., Mitrovica, J.X., Huybers, P., Rovere, A., 2017. Detection of a dynamic topography signal in last interglacial sea-level records. Sci. Adv. 3 (7), e1700457.

Bayarsky, A., Codignotto, J.O., 1982. Pleistoceno- Holoceno marino en Puerto Lobos, Chubut. Rev. Asoc. Geol. Argent. 37 (1), 91–99.

Beuzen, T., Goldstein, E.B., Splinter, K.D., 2019. Ensemble models from machine learning: an example of wave runup and coastal dune erosion. Nat. Hazards Earth Syst. Sci. 19 (10), 2295–2309.

Bini, M., Isola, I., Zanchetta, G., Pappalardo, M., Ribolini, A., Ragaini, L., Baroni, C., Boretto, G., Fuck, E., Morigi, C., et al., 2018. Mid-holocene relative sea-level changes along atlantic Patagonia: new data from Camarones, Chubut, Argentina. Holocene 28 (1), 56–64.

Bird, P., 2003. An updated digital model of plate boundaries. G-cubed 4 (3).

Björck, S., Lambeck, K., Möller, P., Waldmann, N., Bennike, O., Jiang, H., Li, D., Sandgren, P., Nielsen, A.B., Porter, C.T., 2021. Relative sea level changes and glacio-isostatic modelling in the Beagle Channel, Tierra del Fuego, Chile: Glacial and tectonic implications. Quat. Sci. Rev. 251, 106657.

Boretto, G., Consoloni, I., Morán, G.A., Regattieri, E., Gordillo, S., Fucks, E., Zanchetta, G., Dallai, L., 2019. Oxygen stable isotope analyses on *Ameghinomya antiqua* shells: a promising tool for palaeoenvironmental reconstruction along the quaternary patagonian Argentina coast? Alpine and Mediterranean. Quaternary 32 (1), 57–72.

Boretto, G.M., Baranzelli, M.C., Gordillo, S., Consoloni, I., Zanchetta, G., Morán, G., 2014. Shell morphometric variations in a patagonian Argentina clam (*Ameghinomya antiqua*) from the mid-pleistocene (mis 7) to the present. Quat. Int. 352, 48–58.

Bowen, D., 2010. Sea level ~400 000 years ago (MIS 11): analogue for present and future sea-level? Clim. Past 6 (1), 19–29.

Braun, J., 2010. The many surface expressions of mantle dynamics. Nat. Geosci. 3 (12), 825–833.

Carrere, L., Lyard, F., Cancet, M., Guillot, A., Picot, N., 2016. FES2014, a new tidal model–Validation results and perspectives for improvements. presentation to ESA Living Planet Conference.

Chen, F., Friedman, S., Gertler, C.G., Looney, J., O'Connell, N., Sierks, K., Mitrovica, J.X., 2014. Refining estimates of polar ice volumes during the MIS11 interglacial using Sea Level records from South Africa. J. Clim. 27 (23), 8740–8746.

Clark, P.U., He, F., Golledge, N.R., Mitrovica, J.X., Dutton, A., Hoffman, J.S., Dendy, S., 2020. Oceanic forcing of penultimate deglacial and last interglacial sea-level rise. Nature 577 (7792), 660–664.

Codignotto, J., 1983. Depósitos elevados y/o de acreción Pleistoceno-Holoceno en la costa Fueguino-Patagónica. In: Simposio Oscilaciones del nivel del mar durante el último hemiciclo deglacial en la Argentina, pp. 12–26.

Codignotto, J.O., Kokot, R.R., Marcomini, S.C., 1992. Neotectonism and sea-level changes in the coastal zone of Argentina. J. Coast Res. 125–133.

Creel, R.C., Austermann, J., Kopp, R., Khan, N.S., Albrecht, T., Kingslake, J.. Global mean sea level higher than present during the Holocene. https://doi.org/10.3122 3/X5JT11.

Creveling, J.R., Mitrovica, J.X., Clark, P.U., Waelbroeck, C., Pico, T., 2017. Predicted bounds on peak global mean sea level during marine isotope stages 5a and 5c. Quat. Sci. Rev. 163, 193–208. https://doi.org/10.31223/X5JT11.

Darwin, C., 1851. Geological observations on coral reefs, volcanic islands, and on South America: being the geology of the voyage of the Beagle, under the command of Captain Fitzroy, RN, during the years 1832 to 1836. Smith, Elder & Company.

DeConto, R.M., Pollard, D., Alley, R.B., Velicogna, I., Gasson, E., Gomez, N., Sadai, S., Condron, A., Gilford, D.M., Ashe, E.L., et al., 2021. The Paris Climate Agreement and future sea-level rise from Antarctica. Nature 593 (7857), 83–89.

Del Río, C.J., Griffin, M., McArthur, J.M., Martínez, S., Thirlwall, M.F., 2013. Evidence for early Pliocene and late Miocene transgressions in southern Patagonia (Argentina): 87Sr/86Sr ages of the pectinid "Chlamys" actinodes (Sowerby). J. S. Am. Earth Sci. 47, 220–229.

Dumitru, O.A., Austermann, J., Polyak, V.J., Fornós, J.J., Asmerom, Y., Ginés, J., Ginés, A., Onac, B.P., 2019. Constraints on global mean sea level during Pliocene warmth. Nature 574 (7777), 233–236.

Dumitru, O.A., Dyer, B., Austermann, J., Sandstrom, M.R., Goldstein, S.L., D'Andrea, W. J., Cashman, M., Creel, R., Bolge, L., Raymo, M.E., 2023. Last interglacial global mean sea level from high-precision U-series ages of Bahamian fossil coral reefs. Quat. Sci. Rev. 318, 108287.

Dutton, A., Carlson, A.E., Long, A.J., Milne, G.A., Clark, P.U., DeConto, R., Horton, B.P., Rahmstorf, S., Raymo, M.E., 2015. Sea-level rise due to polar ice-sheet mass loss during past warm periods. Science 349 (6244), aaa4019.

Duval, M., Arnold, L.J., Rixhon, G., 2020. Electron spin resonance (ESR) dating in Quaternary studies: evolution, recent advances and applications. Quat. Int. 556, 1–10.

Dyer, B., Austermann, J., D'Andrea, W.J., Creel, R.C., Sandstrom, M.R., Cashman, M., Rovere, A., Raymo, M.E., 2021. Sea-level trends across the Bahamas constrain peak last interglacial ice melt. Proc. Natl. Acad. Sci. USA 118 (33), e2026839118.

Fedorov, A.V., Brierley, C., Lawrence, K.T., Liu, Z., Dekens, P., Ravelo, A., 2013. Patterns and mechanisms of early Pliocene warmth. Nature 496 (7443), 43–49.

Feruglio, E., 1949. Descripción geológica de la Patagonia. Coni Publishing House.

Fox-Kemper, B., Hewitt, H., Xiao, C., Aðalgeirsdóttir, G., Drijfhout, S., Edwards, T., Golledge, N., Hemer, M., Kopp, R., Krinner, G., Mix, A., Notz, D., Nowicki, S., Nurhati, I., Ruiz, L., Sallée, J.-B., Slangen, A., Yu, Y., 2021. Ocean, cryosphere and Sea Level change. In: Masson-Delmotte, V., Zhai, P., Pirani, A., Connors, S.L., Péan, C., Berger, S., Caud, N., Chen, Y., Goldfarb, L., Gomis, M.I., Huang, M., Leitzell, K., Lonnoy, E., Matthews, J.B.R., Maycock, T.K., Waterfield, T., Yelekçi, O., Yu, R., Zhou, B. (Eds.), Climate Change 2021: *the Physical Science Basis. Contribution Of Working Group I to the Sixth Assessment Report Of the Intergovernmental Panel On Climate Change*, Chapter 9. Cambridge University Press, Cambridge, UK and New York, NY, USA.

Gilford, D.M., Ashe, E.L., DeConto, R.M., Kopp, R.E., Pollard, D., Rovere, A., 2020. Could the last interglacial constrain projections of future Antarctic ice mass loss and sealevel rise? J. Geophys. Res.: Earth Surf. 125 (10), e2019JF005418.

Goodfriend, G.A., 1991. Patterns of racemization and epimerization of amino acids in land snail shells over the course of the Holocene. Geochem. Cosmochim. Acta 55 (1), 293–302.

Gordillo, S., 1999. Holocene molluscan assemblages in the magellan region. Sci. Mar. 63 (S1), 15–22.

Gowan, E.J., Rovere, A., Ryan, D.D., Richiano, S., Montes, A., Pappalardo, M., Aguirre, M.L., 2021a. Last interglacial (MIS 5e) sea-level proxies in southeastern South America. Earth Syst. Sci. Data 13 (1), 171–197.

Gowan, E.J., Zhang, X., Khosravi, S., Rovere, A., Stocchi, P., Hughes, A.L., Gyllencreutz, R., Mangerud, J., Svendsen, J.-I., Lohmann, G., 2021b. A new global ice sheet reconstruction for the past 80 000 years. Nat. Commun. 12 (1), 1199.

Grant, G., Naish, T., Dunbar, G., Stocchi, P., Kominz, M., Kamp, P.J., Tapia, C., McKay, R., Levy, R., Patterson, M., 2019. The amplitude and origin of sea-level variability during the Pliocene epoch. Nature 574 (7777), 237–241.

Gulev, S., Thorne, P., Ahn, J., Dentener, F., Domingues, C., Gerland, S., Gong, D., Kaufman, D., Nnamchi, H., Quaas, J., Rivera, J., Sathyendranath, S., Smith, S., Trewin, B., von Schuckmann, K., Vose, R., 2021. Climate Change 2021: *the Physical Science Basis. Contribution Of Working Group I to the Sixth Assessment Report Of the Intergovernmental Panel On Climate Change*, Chapter 2. Cambridge University Press, Cambridge, UK and New York, NY, USA, pp. 287–422.

Hay, C., Mitrovica, J.X., Gomez, N., Creveling, J.R., Austermann, J., E. Kopp, R., 2014. The sea-level fingerprints of ice-sheet collapse during interglacial periods. Quat. Sci. Rev. 87, 60–69.

Hearty, P.J., Kindler, P., Cheng, H., Edwards, R., 1999. A+ 20 m middle Pleistocene sea-level highstand (Bermuda and the Bahamas) due to partial collapse of Antarctic ice. Geology 27 (4), 375–378.

Heaton, T.J., Köhler, P., Butzin, M., Bard, E., Reimer, R.W., Austin, W.E.N., Bronk Ramsey, C., Grootes, P.M., Hughen, K.A., Kromer, B., et al., 2020. Marine20—the marine radiocarbon age calibration curve (0–55,000 cal BP). Radiocarbon 62 (4), 779–820.

Hillaire-Marcel, C., Gariépy, C., Ghaleb, B., Goy, J.-L., Zazo, C., Cuerda Barcelo, J., 1996. U-series measurements in tyrrhenian deposits from mallorca —further evidence for two last-interglacial high sea levels in the Balearic Islands. Quat. Sci. Rev. 15 (1), 53–62.

Hollyday, A., Austermann, J., Lloyd, A., Hoggard, M., Richards, F., Rovere, A., 2023. A revised estimate of early Pliocene global mean Sea Level using geodynamic models of the patagonian slab window. G-cubed 24 (2), e2022GC010648.

Holman, R., 1986. Extreme value statistics for wave run-up on a natural beach. Coast. Eng. 9 (6), 527–544.

IMOS, 2023. Imos - SRS Surface Waves Sub-Facility – altimeter wave/wind. Technical Report, Australia's Integrated Marine Observing System (IMOS).

Jedoui, Y., Reyss, J.-L., Kallel, N., Montacer, M., Ismaïl, H.B., Davaud, E., 2003. U-series evidence for two high Last Interglacial sea levels in southeastern Tunisia. Quat. Sci. Rev. 22 (2), 343–351.

Kaufman, D.S., Manley, W.F., 1998. A new procedure for determining dl amino acid ratios in fossils using reverse phase liquid chromatography. Quat. Sci. Rev. 17 (11), 987–1000.

Khan, N.S., Hibbert, F., Rovere, A., 2019a. sea-level databases. Past Global Changes Magazine 27, 10–11.

Khan, N.S., Horton, B.P., Engelhart, S., Rovere, A., Vacchi, M., Ashe, E.L., Törnqvist, T.E., Dutton, A., Hijma, M.P., Shennan, I., 2019b. Inception of a global atlas of sea levels since the Last Glacial Maximum. Quat. Sci. Rev. 220, 359–371.

Kosnik, M.A., Kaufman, D.S., 2008. Identifying outliers and assessing the accuracy of amino acid racemization measurements for geochronology: II. Data screening. Quat. Geochronol. 3 (4), 328–341.

Labonne, M., Hillaire-Marcel, C., 2000. Geochemical gradients within modern and fossil shells of Concholepas concholepas from northern Chile: an insight into U–Th systematics and diagenetic/authigenic isotopic imprints in mollusk shells. Geochem. Cosmochim. Acta 64 (9), 1523–1534.

Lamothe, M., 2016. Luminescence dating of interglacial coastal depositional systems: recent developments and future avenues of research. Quat. Sci. Rev. 146, 1–27.

Leaman, C., Beuzen, T., Goldstein, E.B., 2020. Chrisleaman/Py-Wave-Runup: V0, 1.10.

Lorscheid, T., Rovere, A., 2019. The indicative meaning calculator–quantification of paleo sea-level relationships by using global wave and tide datasets. Open Geospatial Data, Software and Standards 4, 1–8.

Lyard, F.H., Allain, D.J., Cancet, M., Carrère, L., Picot, N., 2021. FES2014 global ocean tide atlas: design and performance. Ocean Sci. 17 (3), 615–649.

Marra, F., Florindo, F., Gaeta, M., Jicha, B., 2023. 40Ar/39Ar age constraints on MIS 5.5 and MIS 5.3 paleosea levels: implications for global sea levels and ice-volume estimates. Paleoceanogr. Paleoclimatol., e2023PA004679

Milne, G.A., Long, A.J., Bassett, S.E., 2005. Modelling holocene relative sea-level observations from the caribbean and south America. Quat. Sci. Rev. 24 (10–11), 1183–1202.

Mitrovica, J., Milne, G., 2002. On the origin of late Holocene sea-level highstands within equatorial ocean basins. Quat. Sci. Rev. 21 (20), 2179–2190.

Mitrovica, J.X., Milne, G.A., Davis, J.L., 2001. Glacial isostatic adjustment on a rotating earth. Geophys. J. Int. 147 (3), 562–578.

Muhs, D.R., Simmons, K.R., Schumann, R.R., Groves, L.T., Mitrovica, J.X., Laurel, D., 2012. Sea-level history during the Last Interglacial complex on San Nicolas Island, California: implications for glacial isostatic adjustment processes, paleozoogeography and tectonics. Quat. Sci. Rev. 37, 1–25.

Murray-Wallace, C.V., 2002. Pleistocene coastal stratigraphy, sea-level highstands and neotectonism of the southern Australian passive continental margin—a review. J. Quat. Sci. 17 (5–6), 469–489.

Naish, T., Powell, R., Levy, R., Wilson, G., Scherer, R., Talarico, F., Krissek, L., Niessen, F., Pompilio, M., Wilson, T., et al., 2009. Obliquity-paced Pliocene West Antarctic ice sheet oscillations. Nature 458 (7236), 322–328.

Nielsen, P., 2009. Coastal and Estuarine Processes, ume 29. World Scientific Publishing Company.

Olson, S.L., Hearty, P.J., 2009. A sustained + 21 m sea level highstand during MIS 11 (400 ka): direct fossil and sedimentary evidence from Bermuda. Quat. Sci. Rev. 28 (3–4), 271–285.

Pappalardo, M., Aguirre, M.L., Bini, M., Consoloni, I., Fucks, E.E., Hellstrom, J., Isola, I., Ribolini, A., Zanchetta, G., 2015. Coastal landscape evolution and sea-level change: a case study from Central Patagonia (Argentina). Zeitschrift für Geomorphologie 59 (2), 145–172. https://doi.org/10.1127/0372-8854/2014/0142.

Pappalardo, M., Baroni, C., Bini, M., Isola, I., Ribolini, A., Salvatore, M.C., Zanchetta, G., 2019. Challenges in relative sea-level change assessment highlighted through a case study: the central coast of atlantic patagonia. Global Planet. Change 182, 103008.

Passarella, M., Goldstein, E.B., De Muro, S., Coco, G., 2018. The use of genetic programming to develop a predictor of swash excursion on sandy beaches. Nat. Hazards Earth Syst. Sci. 18 (2), 599–611.

Pedoja, K., Regard, V., Husson, L., Martinod, J., Guillaume, B., Fucks, E., Iglesias, M., Weill, P., 2011. Uplift of Quaternary shorelines in eastern Patagonia: Darwin revisited. Geomorphology 127 (3–4), 121–142.

Peltier, W.R., 2002. Global glacial isostatic adjustment: palaeogeodetic and space-geodetic tests of the ICE-4G (VM2) model. J. Quat. Sci. 17 (5–6), 491–510.

Peltier, W.R., Argus, D., Drummond, R., 2015. Space geodesy constrains ice age terminal deglaciation: the global ICE-6G_C (VM5a) model. J. Geophys. Res. Solid Earth 120 (1), 450–487.

Piñón, D., Zhang, K., Wu, S., Cimbaro, S., 2018. A new argentinean gravimetric geoid model: GEOIDEAR. In: International Symposium on Earth and Environmental Sciences for Future Generations: Proceedings of the IAG General Assembly, Prague, Czech Republic, June 22-July 2, 2015. Springer, pp. 53–62.

Polyak, V.J., Onac, B.P., Fornós, J.J., Hay, C., Asmerom, Y., Dorale, J.A., Ginés, J., Tuccimei, P., Ginés, A., 2018. A highly resolved record of relative sea level in the western Mediterranean Sea during the last interglacial period. Nat. Geosci. 11 (11), 860–864.

Raymo, M.E., Mitrovica, J.X., 2012. Collapse of polar ice sheets during the stage 11 interglacial. Nature 483 (7390), 453–456.

Raymo, M.E., Mitrovica, J.X., O'Leary, M.J., DeConto, R.M., Hearty, P.J., 2011. Departures from eustasy in Pliocene sea-level records. Nat. Geosci. 4 (5), 328–332.

Reimer, P.J., Reimer, R.W., 2001. A marine reservoir correction database and on-line Interface. Radiocarbon 43 (2A), 461–463.

Ribolini, A., Aguirre, M., Baneschi, I., Consoloni, I., Fucks, E., Isola, I., Mazzarini, F., Pappalardo, M., Zanchetta, G., Bini, M., 2011. Holocene beach ridges and coastal evolution in the Cabo Raso bay (Atlantic Patagonian coast, Argentina). J. Coast Res. 27 (5), 973–983.

Roberts, D.L., Karkanas, P., Jacobs, Z., Marean, C.W., Roberts, R.G., 2012. Melting ice sheets 400,000 yr ago raised sea level by 13 m: Past analogue for future trends. Earth Planet Sci. Lett. 357, 226–237.

Rojas, A., Martínez, S., 2016. Marine isotope stage 3 (MIS 3) versus marine isotope stage 5 (MIS 5) fossiliferous marine deposits from Uruguay. In: Marine Isotope Stage 3 in Southern South America, 60 KA BP-30 KA BP. Springer, pp. 249–278.

Rostami, K., Peltier, W., Mangini, A., 2000. Quaternary marine terraces, sea-level changes and uplift history of Patagonia, Argentina: comparisons with predictions of the ICE-4G (VM2) model of the global process of glacial isostatic adjustment. Quat. Sci. Rev. 19 (14–15), 1495–1525.

Rovere, A., 2021. GPS-utilities Ver, p. 1.0. https://doi.org/10.5281/zenodo.5169168.

Rovere, A., Pappalardo, M., Richiano, S., Aguirre, M., Sandstrom, M.R., Hearty, P.J., Austermann, J., Castellanos, I., Raymo, M.E., 2020. Higher than present global mean sea level recorded by an Early Pliocene intertidal unit in Patagonia (Argentina). Communications Earth & Environment 1 (1), 68.

Rovere, A., Ryan, D.D., Vacchi, M., Dutton, A., Simms, A.R., Murray-Wallace, C.V., 2023. The world atlas of last interglacial shorelines (version 1.0). Earth Syst. Sci. Data 15 (1), 1–23.

Rovere, A., Stocchi, P., Vacchi, M., 2016. Eustatic and relative sea level changes. Curr. Clim. Change Rep. 2, 221–231.

Rubio-Sandoval, K., Rovere, A., Cerrone, C., Stocchi, P., Lorscheid, T., Felis, T., Petersen, A.-K., Ryan, D.D., 2021. A review of last interglacial sea-level proxies in the western Atlantic and southwestern Caribbean, from Brazil to Honduras. Earth Syst. Sci. Data 13 (10), 4819–4845.

Ruggiero, P., Komar, P.D., McDougal, W.G., Marra, J.J., Beach, R.A., 2001. Wave runup, extreme water levels and the erosion of properties backing beaches. J. Coast Res. 407–419.

Rutter, N., Schnack, E.J., del Rio, J., Fasano, J.L., Isla, F.I., Radtke, U., 1989. Correlation and dating of Quaternary littoral zones along the Patagonian coast, Argentina. Quat. Sci. Rev. 8 (3), 213–234.

Ryan, W.B.F., Carbotte, S.M., Coplan, J.O., O'Hara, S., Melkonian, A., Arko, R., Weissel, R.A., Ferrini, V., Goodwillie, A., Nitsche, F., Bonczkowski, J., Zemsky, R., 2009. Global multi-resolution topography synthesis. G-cubed 10 (3).

Schellmann, G., 1998. Jungkänozoische Landschaftsgeschichte Patagoniens (Argentinien): andine Vorlandvergletscherungen, Talentwicklung und marine Terrassen. 1. Auflage, Essen: Klartext, 1998.

Schellmann, G., Beerten, K., Radtke, U., 2008. Electron sin resonance (ESR) dating of Quaternary materials. E&G Quaternary Science Journal 57 (1/2), 150–178.

Schellmann, G., Radtke, U., 2000. ESR dating stratigraphically well-constrained marine terraces along the Patagonian Atlantic coast (Argentina). Quat. Int. 68, 261–273.

Schellmann, G., Radtke, U., 2003. Coastal terraces and Holocene sea-level changes along the Patagonian Atlantic coast. J. Coast Res. 983–996.

Schellmann, G., Radtke, U., 2007. Neue Befunde zur Verbreitung und chronostratigraphischen Gliederung holozäner Küstenterrassen an der mittel-und südpatagonischen Atlantikküste (Argentinien)–Zeugnisse holozäner Meeresspiegelveränderungen. Bamb. Geogr. Schriften 22, 1–91.

Schellmann, G., Radtke, U., 2010. Timing and magnitude of Holocene sea-level changes along the middle and south Patagonian Atlantic coast derived from beach ridge systems, littoral terraces and valley-mouth terraces. Earth Sci. Rev. 103 (1–2), 1–30.

Schwarcz, H.P., 1994. Current challenges to ESR dating. Quat. Sci. Rev. 13 (5), 601–605.

Scussolini, P., Dullaart, J., Muis, S., Rovere, A., Bakker, P., Coumou, D., Renssen, H., Ward, P.J., Aerts, J.C.J.H., 2023. Modeled storm surge changes in a warmer world: the last interglacial. Clim. Past 19 (1), 141–157.

Senechal, N., Coco, G., Bryan, K.R., Holman, R.A., 2011. Wave runup during extreme storm conditions. J. Geophys. Res.: Oceans 116 (C7).

Shennan, I., 2015. Handbook of sea-level research: framing research questions. Handbook of Sea-Level Research, pp. 3–25.

Siddall, M., Chappell, J., Potter, E.-K., 2007. 7. Eustatic sea level during past interglacials. In: Developments in Quaternary Sciences, ume 7. Elsevier, pp. 75–92.

Simms, A.R., Rouby, H., Lambeck, K., 2016. Marine terraces and rates of vertical tectonic motion: the importance of glacio-isostatic adjustment along the Pacific coast of central North America. Bulletin 128 (1–2), 81–93.

Smith, C., Salles, T., Concejo, A.V.. pyReefmodel/RADWave: RADWave: Python code for ocean surface wave analysis by satellite radar altimeter. https://doi.org/10.5281/zenodo.3733848.

Solgaard, A.M., Reeh, N., Japsen, P., Nielsen, T., 2011. Snapshots of the Greenland ice sheet configuration in the Pliocene to early Pleistocene. J. Glaciol. 57 (205), 871–880.

Stockdon, H.F., Holman, R.A., Howd, P.A., Sallenger, A.H., 2006. Empirical parameterization of setup, swash, and runup. Coast. Eng. 53 (7), 573–588.

Styron, R., 2019. GEMScienceTools/gem-global-active-faults: First release of 2019. https://doi.org/10.5281/zenodo.3376300.

Tawil-Morsink, K., Austermann, J., Dyer, B., Dumitru, O.A., Precht, W.F., Cashman, M., Goldstein, S.L., Raymo, M.E., 2022. Probabilistic investigation of global mean sea level during MIS 5a based on observations from Cave Hill, Barbados. Quaternary Science Reviews 295, 107783.

Thompson, S.B., Creveling, J.R., 2021. A global database of marine isotope substage 5a and 5c marine terraces and paleoshoreline indicators. Earth Syst. Sci. Data 13 (7), 3467–3490.

Tzedakis, P.C., Hodell, D.A., Nehrbass-Ahles, C., Mitsui, T., Wolff, E.W., 2022. Marine isotope stage 11c: an unusual interglacial. Quat. Sci. Rev. 284, 107493.

US Geological Survey, Earthquake Hazards Program, 2017. Advanced National Seismic System (ANSS) comprehensive catalog of earthquake events and products: Various.

Van de Plassche, O., 1986. Sea-Level research: a manual for the collection and evaluation of data. Geobooks (Norwich).

van de Wal, R.S., Nicholls, R.J., Behar, D., McInnes, K., Stammer, D., Lowe, J.A., Church, J.A., DeConto, R., Fettweis, X., Goelzer, H., et al., 2022. A high-end estimate of Sea Level rise for practitioners. Earth's Future 10 (11), e2022EF002751.

Vos, K., Harley, M.D., Splinter, K.D., Walker, A., Turner, I.L., 2020. Beach slopes from satellite-derived shorelines. Geophys. Res. Lett. 47 (14), e2020GL088365.

Vos, K., Splinter, K.D., Harley, M.D., Simmons, J.A., Turner, I.L., 2019. CoastSat: a Google Earth Engineenabled Python toolkit to extract shorelines from publicly available satellite imagery. Environ. Model. Software 122, 104528.

Vousdoukas, M.I., Wziatek, D., Almeida, L.P., 2012. Coastal vulnerability assessment based on video wave runup observations at a mesotidal, steep-sloped beach. Ocean Dynamics 62, 123–137.

Wehmiller, J.F., 1982. A review of amino acid racemization studies in Quaternary mollusks: stratigraphic and chronologic applications in coastal and interglacial sites, pacific and Atlantic coasts, United States, United Kingdom, baffin Island, and tropical islands. Quat. Sci. Rev. 1 (2), 83–120.

Wehmiller, J.F., 2013a. Interlaboratory comparison of amino acid enantiomeric ratios in Pleistocene fossils. Quat. Geochronol. 16, 173–182.

Wehmiller, J.F., 2013b. United States Quaternary coastal sequences and molluscan racemization geochronology – what have they meant for each other over the past 45 years? Quat. Geochronol. 16, 3–20.

Wehmiller, J.F., Miller, G.H., 2000. Aminostratigraphic Dating Methods in Quaternary Geology. American Geophysical Union (AGU), pp. 187–222.

Yousefi, M., Milne, G., Li, S., Wang, K., Bartholet, A., 2020. Constraining interseismic deformation of the cascadia subduction zone: new insights from estimates of vertical land motion over different timescales. J. Geophys. Res. Solid Earth 125 (3), e2019JB018248.

Zanchetta, G., Consoloni, I., Isola, I., Pappalardo, M., Ribolini, A., Aguirre, M., Fucks, E., Baneschi, I., Bini, M., Ragaini, L., et al., 2012. New insights on the holocene marine transgression in the bahía Camarones (chubut, Argentina). Italian Journal of Geosciences 131 (1), 19–31.

GEBCO, Bathymetric Compilation Group, 2023. The GEBCO_2023 Grid - a continuous terrain model of the global oceans and land. doi:10.5285/1c44ce99-0a0d-5f4f-e063-7086abc0ea0f.